ENGINEERING RESEARCH INSTITUTE
UNIVERSITY OF MICHIGAN
ANN ARBOR

A NEW SINGLE-CAVITY RESONATOR

FOR

A MULTIANODE MAGNETRON

Technical Report No. 6

Electron Tube Laboratory

Department of Electrical Engineering

BY

J. S. NEEDLE

G. HOK

Approved by: W. G. DOW

Project M762

CONTRACT NO. W-36-039 sc-35561
SIGNAL CORPS, DEPARTMENT OF THE ARMY
DEPARTMENT OF ARMY PROJECT NO.339-13-022
SIGNAL CORPS PROJECT NO.112B-0

January 8, 1951

ABSTRACT

This report presents theory and experimental results pertaining to the operation of a new single-cavity resonator magnetron designed for operation at a wave length of 14 centimeters. Power output of 165 watts C-W at 55 per cent efficiency has been attained from one of several tubes built at the University of Michigan Electron Tube Laboratory. The geometry of the structure employed in this magnetron results in an inherent unbalance of r-f potential differences between the cathode and the anode sets of opposite phase in the π mode of operation. Experimental results show that good electronic efficiency is possible even though an appreciable r-f voltage unbalance (more than 25 to 1) exists. However, the maximum-current boundary for the tubes built so far is not as large as it should be with the available emission. The single-cavity resonator employed in this tube is capable of wide-range tunability, as well as parallel operation of several anode structures with a maximum of mode separation. The tubes constructed to date have been of the nontunable variety. A tunable magnetron of this type is now in the process of development.

ACKNOWLEDGEMENTS

Many members of the staff of the University of Michigan Electron Tube Laboratory were engaged in the work which made this report possible. The details of design and construction were the responsibility of Messrs. H. W. Welch, Jr., and J. R. Black. Experimental data were made available mainly through the efforts of Mr. G. R. Brewer. The fabrication of tube parts was done by Messrs. T. G. Keith and R. F. Denning under the supervision of Mr. V. R. Burris, and the drawings were made by Mr. N. Navarre. Tube assembly was the work of Messrs. R. F. Steiner and J. W. VanNatter.

TABLE OF CONTENTS

MAJOR REPORTS ISSUED TO DATE

Contract No. W-36-039 sc-32245. Subject: Theoretical Study, Design and Construction of C-W Magnetrons for Frequency Modulation.

Technical Report No. 1 --

H. W. Welch, Jr. "Space-Charge Effects and Frequency Characteristics of C-W Magnetrons Relative to the Problem of Frequency Modulation", November 15, 1948.

Technical Report No. 2 --

H. W. Welch, Jr., G. R. Brewer. "Operation of Interdigital Magnetrons in the Zero Order Mode", May 23, 1949.

Technical Report No. 3 --

H. W. Welch, Jr., J. R. Black, G. R. Brewer, G. Hok. "Final Report", May 27, 1949.

Contract No. W-36-039 sc-35561. Subject: Theoretical Study, Design and Construction of C-W Magnetrons for Frequency Modulation.

Interim Report --

H. W. Welch, Jr., J. R. Black, G. R. Brewer. December 15, 1949.

Quarterly Report No. 1 --

H. W. Welch, Jr., J. R. Black, G. R. Brewer, G. Hok. April, 1950.

Quarterly Report No. 2 --

H. W. Welch, Jr., J. R. Black, G. R. Brewer, J. S. Needle, W. Peterson. July, 1950.

Quarterly Report No. 3 --

H. W. Welch, Jr., J. R. Black, J. S. Needle, H. W. Batten, G. R. Brewer, W. Peterson, S. Ruthberg. September, 1950.

Technical Report No. 4 --

H. W. Welch, Jr. "Effects of Space Charge on Frequency Characteristics of Magnetrons", Proc. IRE, 38, 1434-1449, December, 1950.

Technical Report No. 5 --

H. W. Welch, Jr., S. Ruthberg, H. W. Batten, W. Peterson. "Dynamic Characteristics of the Magnetron Space Charge", December, 1950.

A NEW SINGLE-CAVITY RESONATOR

FOR

A MULTIANODE MAGNETRON

1. INTRODUCTION

A new multianode, single-cavity resonator magnetron designed for nontunable C-W operation at 14 centimeters has been under investigation at the University of Michigan Electron Tube Laboratory.* Power output of 165 watts with an overall efficiency of 55 per cent and an electronic efficiency of 61 per cent has been attained from one of a number of tubes built. C-W performance data on three tubes and pulsed performance traces for two tubes are included in the experimental results.

An unbalance (more than 25 to 1) of r-f potential differences between the cathode and the anode segments of opposite phase (in π-mode operation) results from the inherent geometry of this new structure. Further discussion of the cathode unbalance and the related problem of power loss through the cathode line is presented in Section 7, Cathode Structures.

The single-cavity resonator magnetron, which has been designated as Model 7, consists of a section of coaxial transmission line excited at its center by an r-f voltage produced between a system of radial vane anodes and longitudinal bar anodes. The radial vane anodes extend inward from the outer conductor of the coaxial line and protrude through slots

---

* This structure was proposed in Technical Report No. 2 (page 50), of this project.

bounded by longitudinal bar anodes in the center conductor. The cathode is located symmetrically within the center conductor. The essential features of the resonator geometry are illustrated in the assembly drawing of Fig. 1.1, and a photograph of one of the tubes is reproduced in Fig. 1.2. Sections 3 and 4 of this report deal with the analysis and design of the resonator.

The Model 7 single-cavity resonator magnetron possesses certain advantages over most existing structures. A few of these advantages are:

(a) The resonator can easily be designed for wide-range tunability.

(b) The dimensions and shape of the resonator can be materially altered without changing the interaction-space design.

(c) Parallel operation of anode structures is possible with a maximum of mode separation.

(d) The basic geometry of the structure is readily adaptable to external-cavity magnetron construction.*

2. INTERACTION-SPACE DESIGN

The region of interaction between the electrons and the r-f field is located within the center conductor at its midpoint. For π-mode operation the bars of the center conductor form one set of anodes and the vanes the other. The design of the interaction space is based on conventional procedures. For the Model 7 tubes the interaction space parameters are as follows:

---

* Quarterly Progress Report No. 3, page 56.

DWG. NO. B

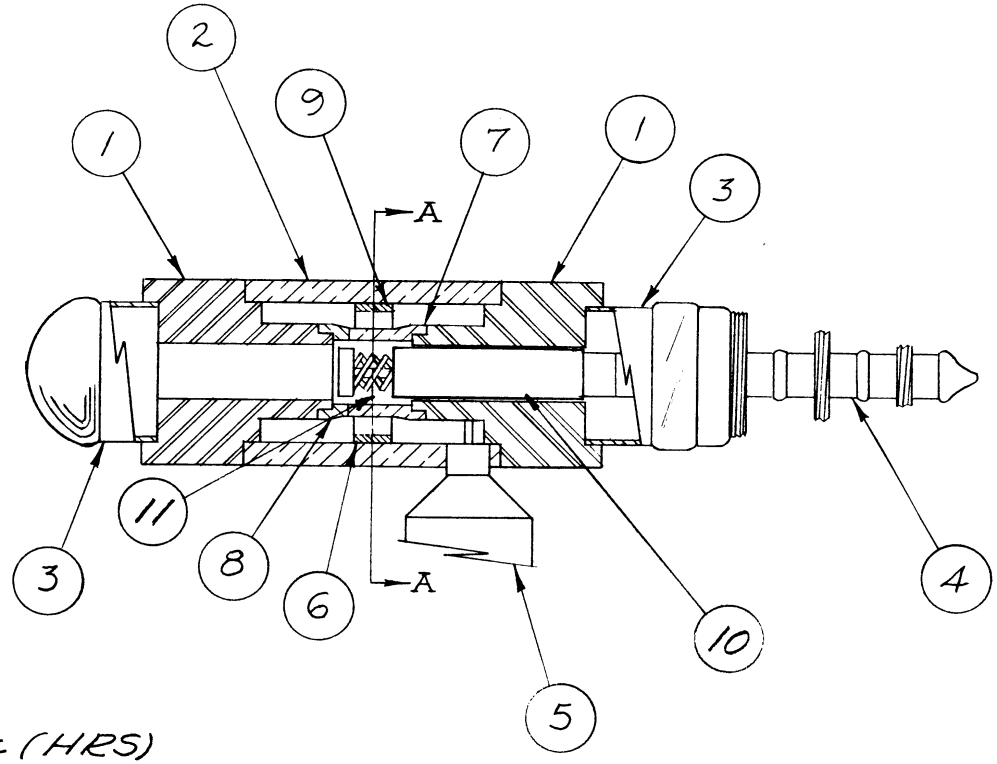

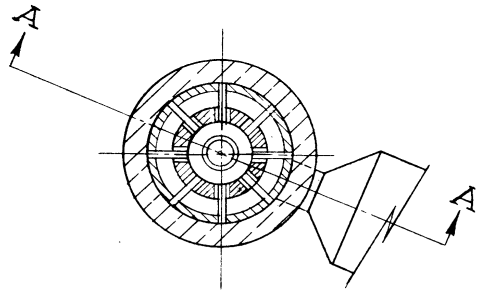

SECTION A-A

1 - POLE PIECE (HRS)
2 - CAVITY SHELL (Cu)
4 - CATHODE CONNECTIONS
5 - OUTPUT PIPE
6 - FILLER RING (FOR MODE SEPARATION)
7 - CAVITY CENTER CONDUCTOR
10 - CATHODE LINE BY-PASS
11 - INTERACTION SPACE

FIG. 1.1

1"

3

ALL DIMENSIONS UNLESS OTHERWISE SPECIFIED MUST BE HELD TO A TOLERANCE - FRACTIONAL ± 1/64," DECIMAL ± .005," ANGULAR ± ½°

ISSUE	DATE			
		ENGINEERING RESEARCH INSTITUTE UNIVERSITY OF MICHIGAN ANN ARBOR MICHIGAN	DESIGNED BY H.W.W.	APPROVED BY
			DRAWN BY ???	SCALE FULL
			CHECKED BY ?-R-?	DATE 10-24-50
		PROJECT M-762	TITLE CO-AXIAL MAGNETRON MODEL 7B	
		CLASSIFICATION	DWG. NO. B- 10,007B	

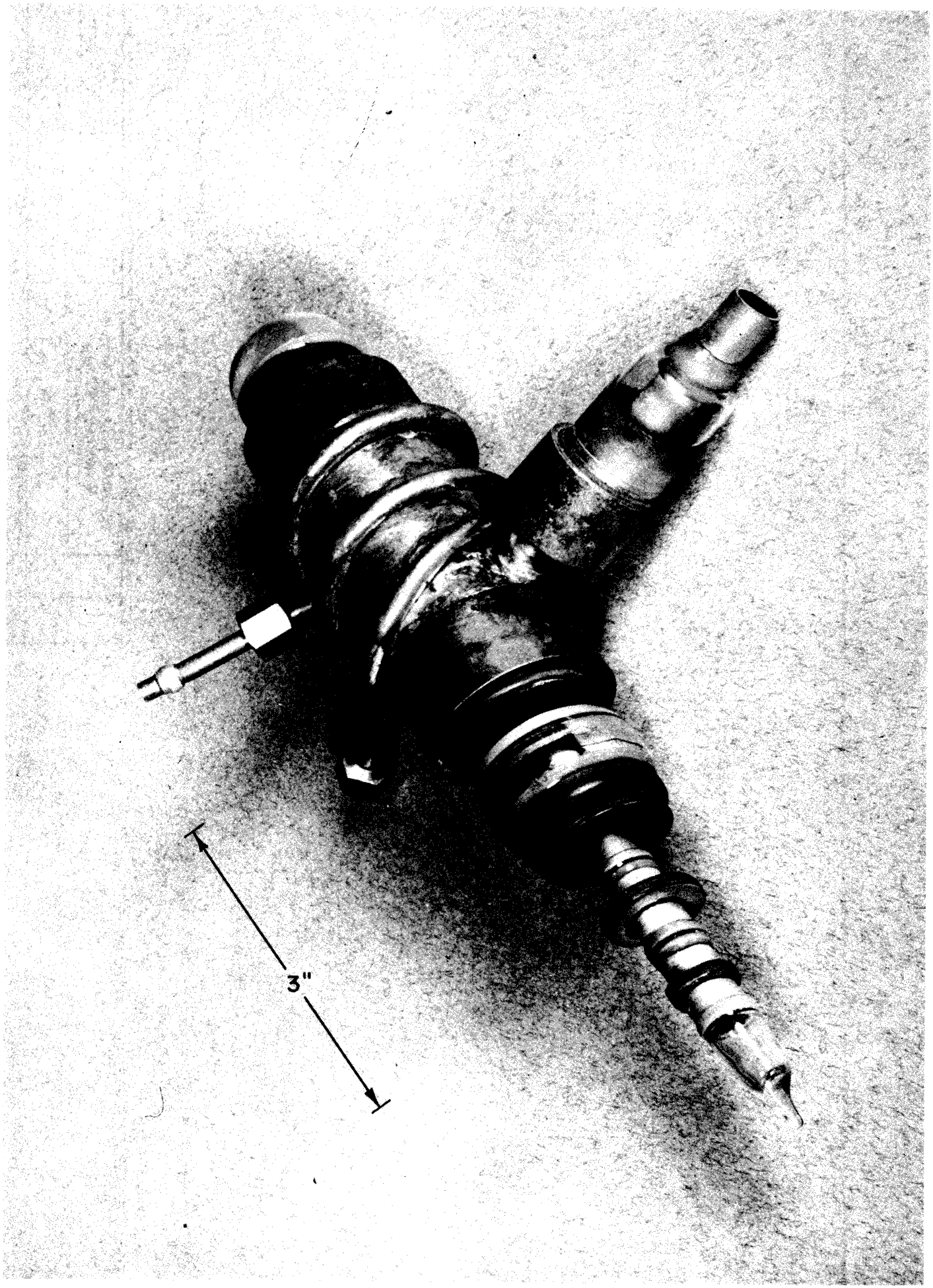

FIG. I.2 PHOTOGRAPH OF COAXIAL SINGLE CAVITY MAGNETRON

λ = 14 cm

N = 16 anodes

r_a = .665 cm = anode radius

r_c = .381 cm = cathode radius

L = .763 cm = length of cathode

r_a/r_c = 1.75 (1.50 has also been used)

V_o = 355 volts

B_o = 286 gauss

where:

$$V_o = \frac{m}{2e}\left(\frac{2\pi c}{n\lambda}\right)^2 r_a^{\,2} \text{ volts} \qquad (n = \frac{N}{2}) \qquad (2.1)$$

$$B_o = \frac{2m}{e}\left(\frac{2\pi c}{n\lambda}\right)\frac{1}{1 - (r_c/r_a)^2} \text{ webers/meter}^2 \qquad (2.2)$$

Typical operation:

V = 3000 volts I = 100 ma.

B = 900 gauss P_o = 100 watts

An axial magnetic field is supplied through copper-plated pole pieces (the parts labeled 1 in Fig. 1.1) which also serve as part of the resonator cavity.

3. RESONATOR DESIGN

The electrical length of the centrally loaded coaxial-line resonator is one-half wave length, where for the models built in this laboratory, λ = 14 centimeters. The design parameters of the resonator structure for operation at a particular frequency are: (a) the capacitance between

the vanes and bars, (b) the inductance of the vanes, (c) the length of the coaxial-line segments, and (d) the output coupling system. Calculations of bar-to-vane capacitance and vane inductance are based on two-dimensional field maps. The field maps themselves are estimated to be correct to within five per cent. The calculated bar-to-vane capacitance is probably correct to within ten per cent. The calculation of vane inductance is based on the assumption of a uniformly distributed current density over the surface of the vane and is therefore only a very rough first approximation. Flux maps and calculations* based on these maps are included in Appendix A. Resonator-design equations and the effect of the output coupling are treated in subsequent sections.

4. RESONATOR-CIRCUIT ANALYSIS

The following approximate analysis was developed in order to determine the equations for (a) the resonance frequency of the cavity, (b) the external Q, and (c) the impedance between the bars and the vanes as seen by the electrons. The analysis is restricted to a lossless cavity resonator in the absence of the cathode. A sketch showing the geometry of the resonator and some of the associated notation is given in Fig. 4.1.

We shall assume that the actual resonator may be represented by a lossless transmission line with lumped constant admittances as in Fig. 4.2. Here Y_L is the load admittance transferred into the coaxial cavity; ℓ_1, ℓ_2, and ℓ_3 are, respectively, the distance of the "T" coupling connection from one shorted end of the coaxial cavity, the distance measured from

---

* Attwood, S. S., Electric and Magnetic Fields. 3rd ed., Chapter 7, Wiley and Sons, New York, 1949.

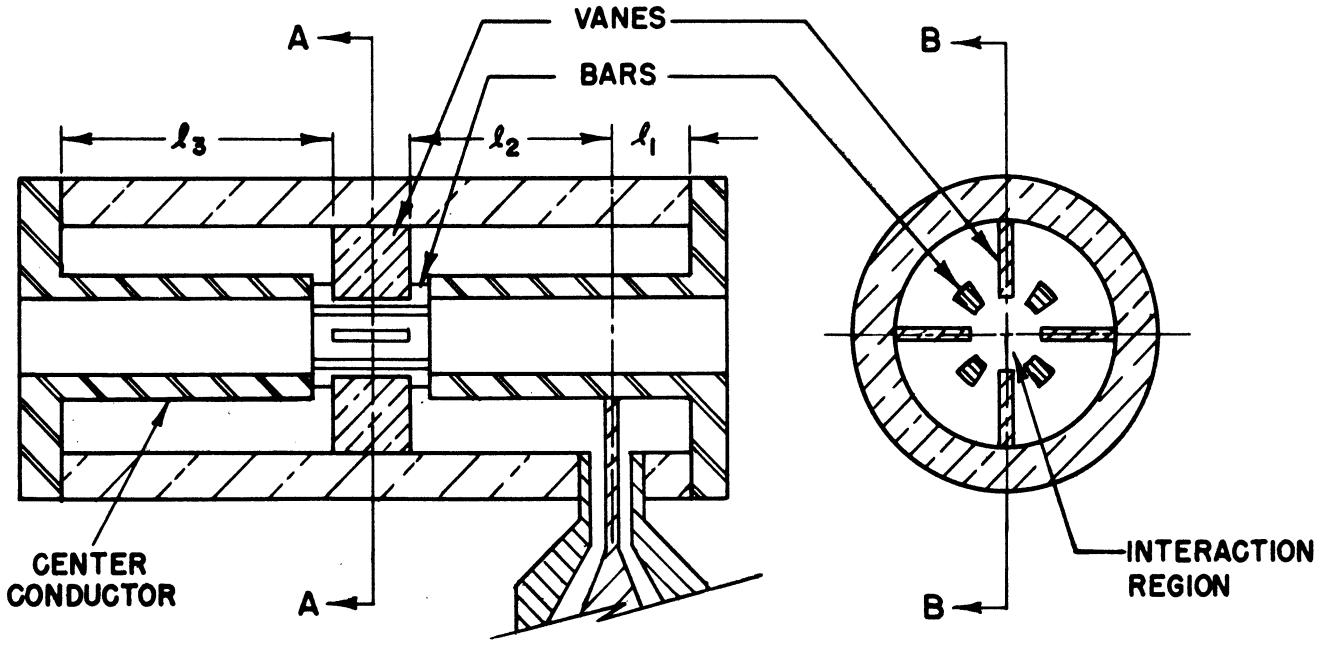

SECTION BB SECTION AA

FIG. 4.1 SKETCH OF MODEL 7 GEOMETRY

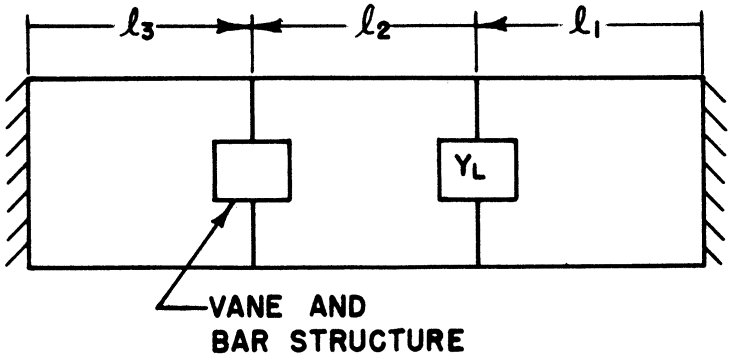

FIG. 4.2
TRANSMISSION LINE EQUIVALENT CIRCUIT

the "T" to the right edge of the vanes, and the distance from the remaining short-circuited end of the coaxial line to the left edge of the vanes.

For convenience in handling, the schematic circuit of Fig. 4.2 is divided into separate components as shown in Fig. 4.3. The admittances indicated on the diagrams define the notations used in the equations which follow.

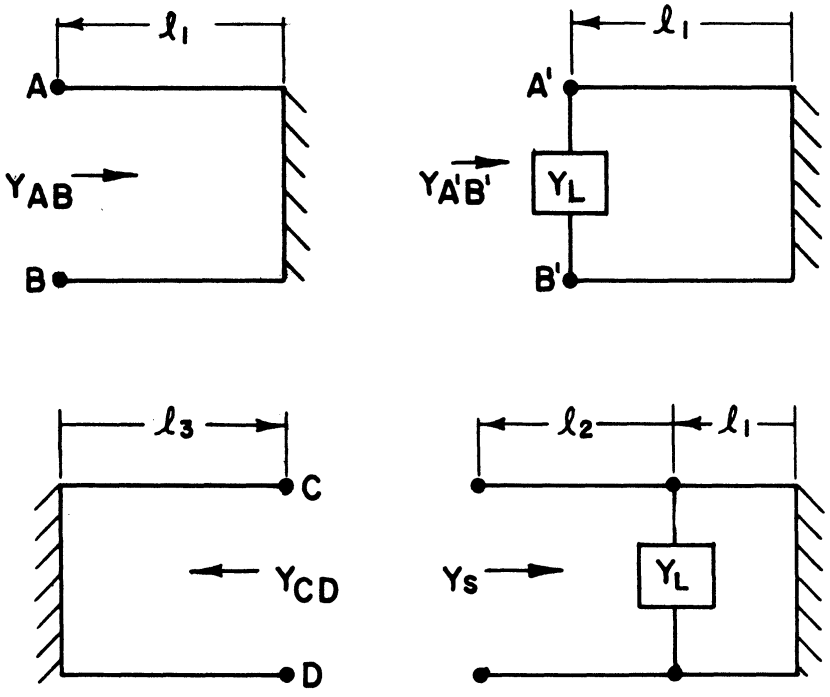

FIG. 4.3

Substituting into the equations for lossless transmission lines, we obtain

$$\frac{Y_S}{Y_0} = \frac{(Y_{AB} + Y_L) + j\, Y_0 \tan \beta \ell_2}{Y_0 + j\,(Y_{AB} + Y_L) \tan \beta \ell_2} \qquad (4.1)$$

$$\frac{Y_{CD}}{Y_0} = -j \cot \frac{2\pi \ell_3}{\lambda}, \qquad Y_{AB} = -j Y_0 \cot \frac{2\pi \ell_1}{\lambda}. \quad (4.2)$$

Let $Y' = Y_S + Y_{CD}$; then

$$\frac{Y'}{Y_0} = \frac{Y_L - j Y_0 \cot(2\pi \ell_1/\lambda) + j Y_0 \tan(2\pi \ell_2/\lambda)}{Y_0 + j \left[Y_L - j Y_0 \cot(2\pi \ell_1/\lambda)\right] \tan \beta \ell_2} - j \cot \frac{2\pi \ell_3}{\lambda}. \quad (4.3)$$

Let

$$\theta_1 = \frac{2\pi \ell_1}{\lambda}, \qquad \theta_2 = \frac{2\pi \ell_2}{\lambda}, \qquad \theta_3 = \frac{2\pi \ell_3}{\lambda}; \quad (4.4)$$

then

$$\frac{Y'}{Y_0} = \frac{Y_L + j Y_0 (\tan \theta_2 - 1/\tan \theta_1)}{Y_0 (1 + \tan \theta_2/\tan \theta_1) + j Y_L \tan \theta_2} - j \frac{1}{\tan \theta_3}. \quad (4.5)$$

Eq 4.5 represents the normalized admittance of the equivalent circuit shown in Fig. 4.4, where Y' is the admittance of the coaxial cavity plus load at the position of the bar and vane structure.

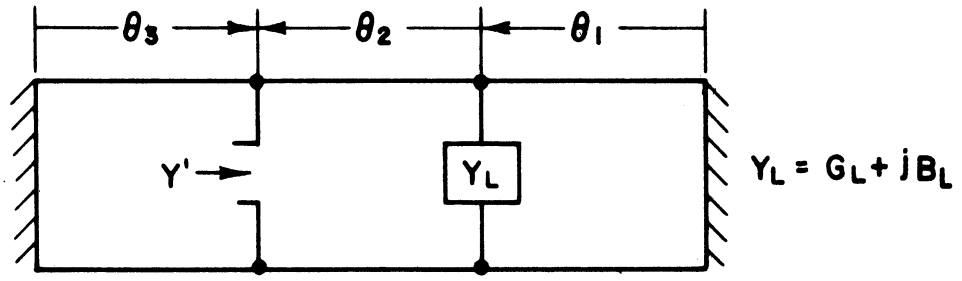

FIG. 4.4

We now consider the effects of the vane and bar geometry as employed in the Model 7 type magnetron. Fig. 4.5 defines the required notation which is used in the equations.

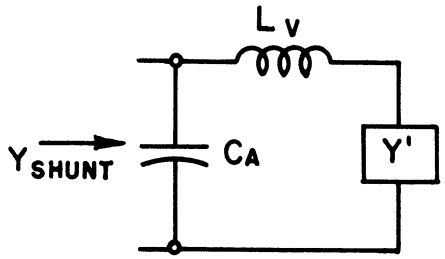

FIG. 4.5

Here L_V is the total inductance of all the vanes in parallel, and C_A is the total capacitance between the vanes and bars. The shunt admittance which is seen by the electrons is:

$$Y_{shunt} = \frac{Y'}{1 + j\omega Y' L_V} + j\omega C_A \, . \qquad (4.6)$$

Substitution of Eq 4.5 for Y' into Eq 4.6 and rationalization results in the expressions given by Eqs 4.8 and 4.9, where

$$\begin{aligned} a &= \tan\theta_1 & \alpha &= (1 + \tfrac{b}{d}) & \beta &= (b - \tfrac{1}{a} - \tfrac{1}{d} - \tfrac{b}{ad}) \\ b &= \tan\theta_2 & & & & \\ d &= \tan\theta_3 & \gamma &= (1 + \tfrac{b}{a}) & Y_L &= G_L + j\, B_L \, , \end{aligned} \qquad (4.7)$$

$$G_{shunt} = \frac{Y_0^2\, G_L\, (\alpha\gamma + b\,\beta)}{\left[\omega L_V Y_0 (Y_0\beta + \alpha B_L) - (Y_0\gamma - bB_L)\right]^2 + \left[\omega L_V Y_0 \alpha G_L - bG_L\right]^2} \, . \qquad (4.8)$$

$$B_{shunt} = \omega C_A$$

$$- \left\{ \frac{Y_0^2 \omega L_V \left[(Y_0\beta + \alpha B_L)^2 + \alpha^2 G_L^2 \right] - Y_0 \left[(Y_0\gamma - bB_L)(Y_0\beta + \alpha B_L) - \alpha b G_L^2 \right]}{\left[\omega L_V Y_0 (Y_0\beta + \alpha B_L) - (Y_0\gamma - bB_L) \right]^2 + \left[\omega L_V Y_0 G_L \alpha - bG_L \right]^2} \right\} \qquad (4.9)$$

Eqs 4.8 and 4.9 can be given a simpler approximate form by making use of the inequalities given below, which were determined from numerical computation. The resultant final approximate equations, 4.10 and 4.11, for shunt susceptance and shunt conductance have been checked numerically against the more exact equations, 4.8 and 4.9, and have been found to be correct to within three per cent for the Model 7 geometry coupled to a matched load.

Since

$$\alpha B_L << Y_0 \beta$$

$$b B_L << Y_0 \gamma$$

and $$\left[\omega L_V Y_0 \alpha G_L - bG_L \right]^2 << \left[\omega L_V Y_0 (Y_0\beta + \alpha B_L) - Y_0\gamma - bB_L \right]^2 ,$$

then

$$G_{shunt} \cong \frac{G_L(\alpha\gamma + b\beta)}{\left[\omega L_V Y_0 \beta - \gamma \right]^2} \quad ; \qquad (4.10)$$

also, since

$$(\alpha G_L)^2 << (Y_0\beta + \alpha B_L)^2$$

$$\alpha b G_L^2 << (Y_0\gamma - bB_L)(Y_0\beta + \alpha B_L)$$

$$bB_L << Y_0\gamma$$

and $$\alpha B_L << Y_0\beta ,$$

then $$B_{shunt} \cong \omega C_A - \frac{Y_0 \beta}{(\omega L_V Y_0 \beta - \gamma)} \quad . \tag{4.11}$$

Substitution for the values of α, β, and γ into Eqs 4.10 and 4.11, and inclusion of the relation $(\theta_1 + \theta_2) = \theta_3$, yields:

$$G_{shunt} \cong G_L Z_0^2 \frac{\sin^2\theta_1}{4\cos^2\theta_3} \frac{1}{\left[\omega L_V + (Z_0/2)\tan\theta_3\right]^2} \tag{4.12}$$

$$B_{shunt} \cong \omega C_A - \frac{1}{\omega L_V + (Z_0/2)\tan\theta_3} \quad . \tag{4.13}$$

Eq 4.13, when set equal to zero, gives the condition for resonance, i.e., resonance of the cavity in the absence of the cathode.

To obtain an expression for Q_e for the Model 7 geometry, we assume B_{shunt} varies linearly with wavelength in the region $\omega = \omega_o$ (see Fig. 4.6); then

$$\left(\frac{dB_{sh}}{d\omega}\right)_{\omega=\omega_o} (\omega_1 - \omega_o) = G_{shunt} \tag{4.14}$$

or

$$\frac{1}{G_{sh}} \left(\frac{dB_{sh}}{d\omega}\right)_{\omega=\omega_o} = \frac{1}{\omega_1 - \omega_o} \quad ; \tag{4.15}$$

multiplying both sides of Eq. 4.15 by $\omega_o/2$ yields

$$\frac{\omega_o}{2\,G_{shunt}} \left(\frac{dB_{sh}}{d\omega}\right)_{\omega=\omega_o} = \frac{\omega_o}{2(\omega_1 - \omega_o)} = Q_e \quad . \tag{4.16}$$

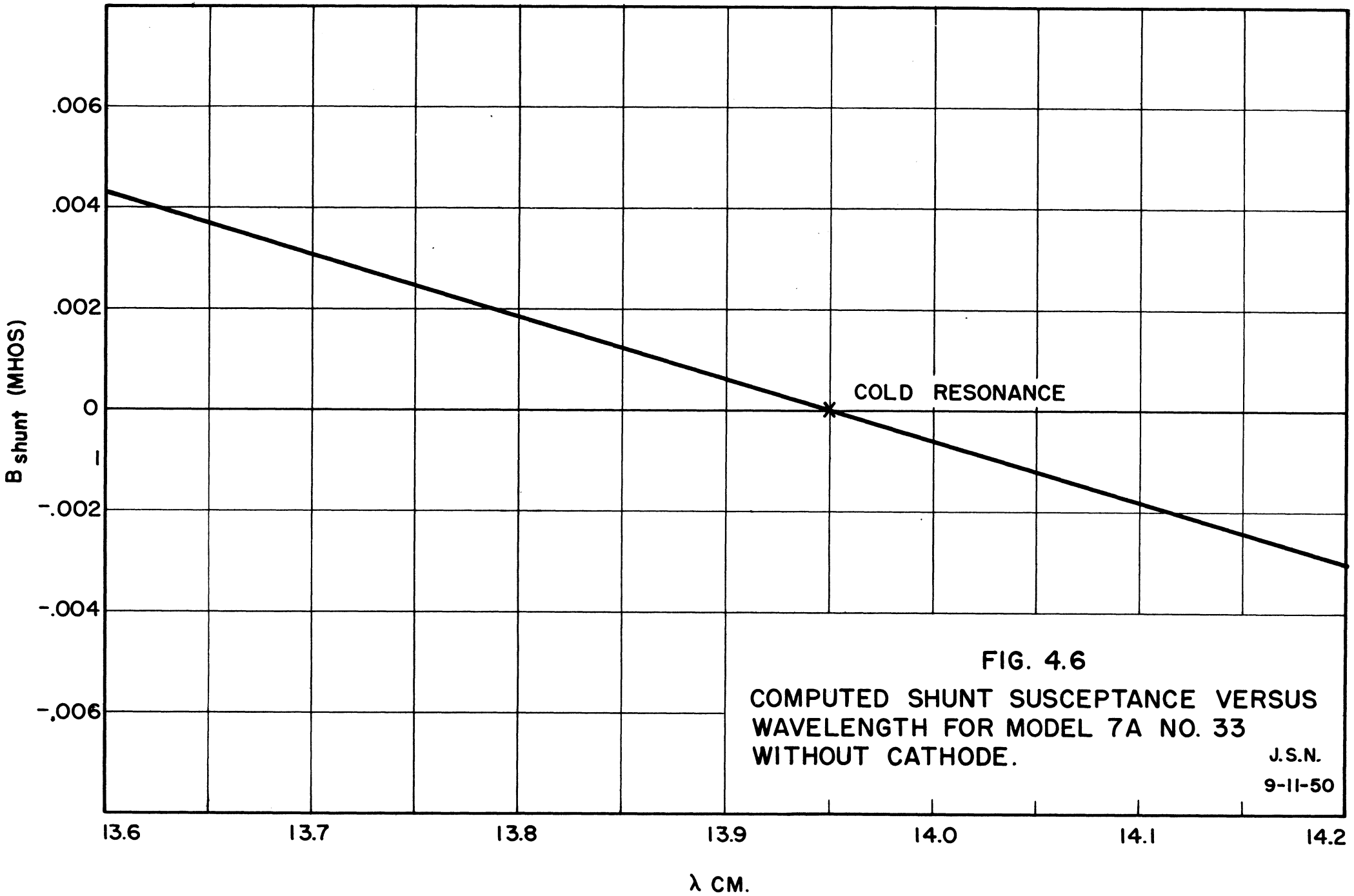

FIG. 4.6

COMPUTED SHUNT SUSCEPTANCE VERSUS WAVELENGTH FOR MODEL 7A NO. 33 WITHOUT CATHODE.

J.S.N.
9-11-50

Carrying out the indicated differentiation, we obtain

$$Q_e = \left\{ C_A + \frac{L_V + (\theta_3 Z_0/2\omega_o)\sec^2\theta_3}{\left[\omega_o L_V + (Z_0/2)\tan\theta_3\right]^2} \right\} \frac{\omega_o}{2\, G_{shunt}} \quad . \tag{4.17}$$

In the case of a "T" coupling to the output line, it can be shown that the load admittance is transferred into the cavity at the position of the "T" with very nearly a one-to-one transformation ratio. The deviation from a one-to-one transformation ratio depends on the load susceptance. The deviation for a matched load in series with the reactance of the coupling geometry used in Model 7 tubes is of the order of three per cent. For the case of the "T" coupling, Eq 4.17, after substitution for G_{shunt}, becomes

$$Q_e = \frac{1}{G_L \sin^2\theta_1} \left[\frac{2\omega_o L_V \cos^2\theta_3}{Z_0^2} + \frac{\omega_o C_A \sin^2\theta_3}{2} + \frac{\theta_3}{Z_0} + \frac{2\omega_o C_A \omega_o L_V \sin\theta_3 \cos\theta_3}{Z_0} \right] . \tag{4.18}$$

A curve of Q_e versus l_1, the distance of the "T" from the cavity wall, is shown in Fig. 5.2.

If we substitute the resonance condition

$$\omega_o C_A = \frac{1}{\omega L_V + (Z_0/2)\tan\theta_3} \tag{4.19}$$

into Eq. 4.17 and then let $\omega_o L_V$ go to zero, we obtain

$$Q_e = \frac{\omega_o C_A}{G_{sh}} \left[\frac{1}{2} + \frac{1}{2} \frac{2\theta_3}{\sin^2\theta_3} \right] \tag{4.20}$$

Eq 4.20 shows the division of energy storage for the Model 7 structure in terms of the lumped energy storage $\omega_o C_A$. Letting θ_3 go to zero in Eq 4.20 results in the relation for Q_e for a lumped constant circuit, i.e.,

$$Q_e = \frac{\omega_o C_A}{G_{sh}} \tag{4.21}$$

5. OUTPUT COUPLING

Fig. 5.1 shows a sketch which gives the details of the output arrangement used in Model 7 tubes. A coupling loop is formed by the length ℓ_1 of the resonator cavity and the section of output-line center conductor, δ, which protrudes into the resonator. The position of the "T" junction relative to the shorted end of the coaxial line, i.e., ℓ_1, determines the relative amount of loading. However, an increase in ℓ_1 increases not only the loading but also the series reactance of the coupling loop.

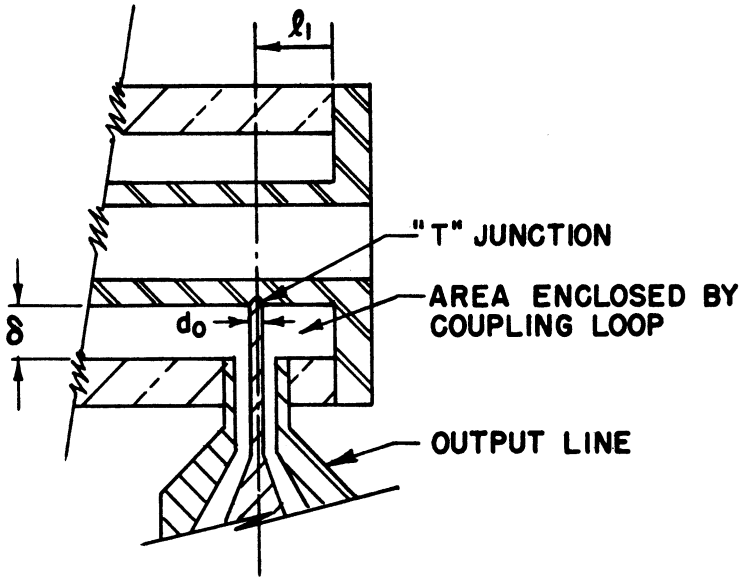

FIG. 5.1

The reactance of the part of the loop formed by the length ℓ_1 of coaxial line is given by $X = Z_o \tan (2\pi\ell_1/\lambda)$. The reactance of the remainder of the coupling loop is estimated on the basis of the inductance of a coaxial transmission line of length δ, whose outer radius is ℓ_1 and whose inner radius is $d_o/2$. The loop reactance is then given approximately by

$$\omega L_\ell = Z_0 \tan \frac{2\pi \ell_1}{\lambda} + \frac{\mu_o}{2\pi} \delta \ln \frac{2\ell_1}{d_o} . \qquad (5.1)$$

The impedance of the load transferred to the position of the "T" inside the cavity (for an output line terminated in its characteristic impedance R_o) is approximately

$$Z_L - R_o + j\omega L_\ell . \qquad (5.2)$$

Fig. 5.2 gives a curve showing the theoretical external Q (see Eq 4.18) as a function of ℓ_1 in per cent of the theoretical external Q of the Model 7A structure. The absolute value of external Q for the Model 7A tube has been calculated to be 160. However, measurements show the actual Q_e to be 340. For this reason, the graph shows the relative rather than the absolute Q_e, so that this empirical value (340) can be extrapolated to any distance ℓ_1.

6. NUMERICAL RESULTS FOR THE MODEL 7A MAGNETRON

In order to find numerical answers for resonant wave length, shunt impedance at resonance, and external Q, certain quantities need to be obtained from the geometry of the resonator, the excitation structure, and the coupling system. These quantities, which are listed below, were approximated by employing two-dimensional field plots.

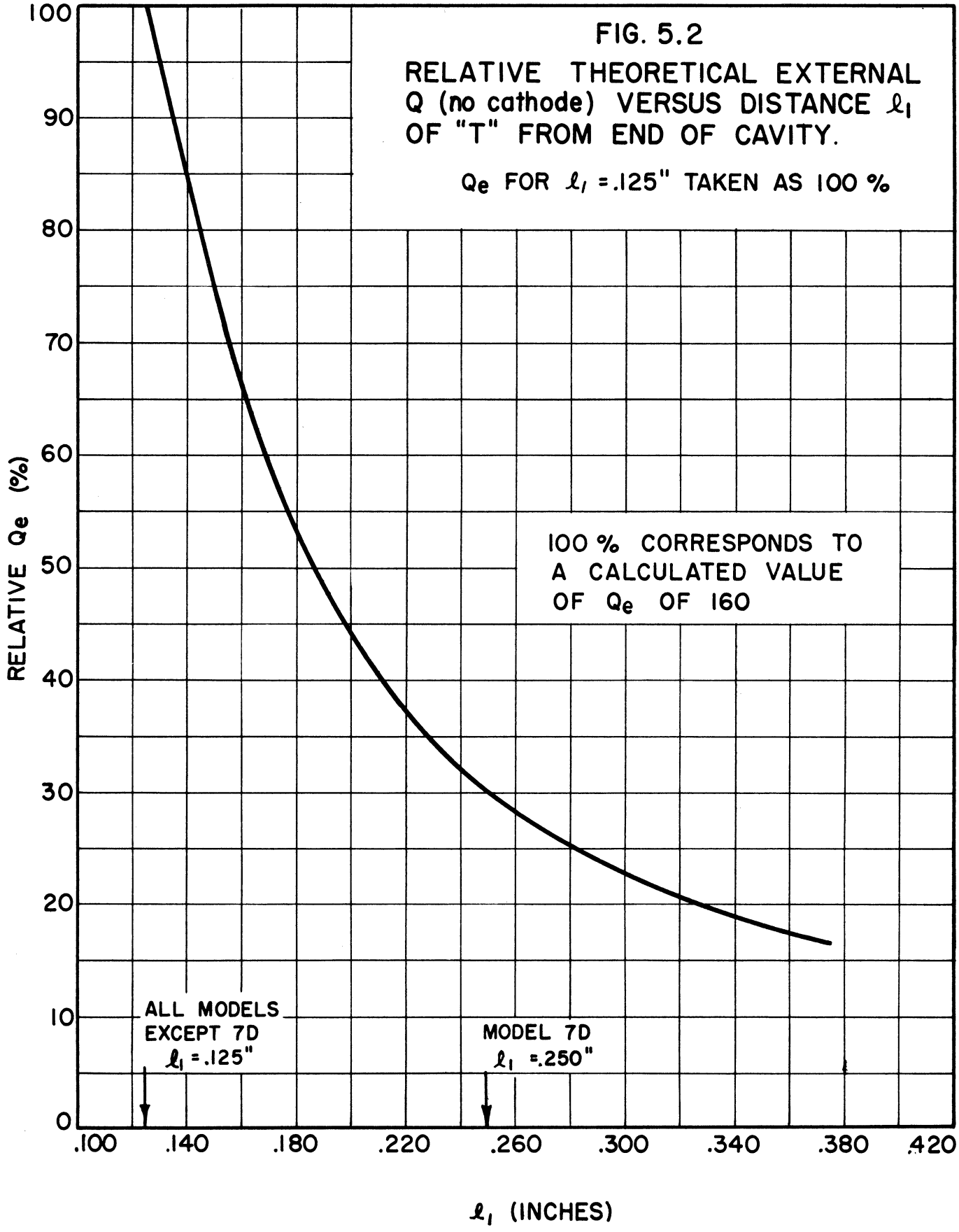
FIG. 5.2
RELATIVE THEORETICAL EXTERNAL Q (no cathode) VERSUS DISTANCE ℓ_1 OF "T" FROM END OF CAVITY.
Q_e FOR ℓ_1 = .125" TAKEN AS 100 %
100 % CORRESPONDS TO A CALCULATED VALUE OF Q_e OF 160
ALL MODELS EXCEPT 7D ℓ_1 = .125"
MODEL 7D ℓ_1 = .250"
RELATIVE Q_e (%)
100
90
80
70
60
50
40
30
20
10
0
.100
.140
.180
.220
.260
.300
.340
.380
.420
ℓ_1 (INCHES)

C_A = 4.88 $\mu\mu$f (total vane-to-bar capacitance)

L_V = 122.9 $\mu\mu$henries (vane inductance — 8 vanes in parallel)

L = 800 $\mu\mu$henries (series inductance of the output-line portion of the "T" connection)

Listed below are the quantities necessary for numerical solution of the circuit equations. These values are computed for 14 cm.

θ_1 = 8.14° θ_3 = 47.5°

θ_2 = 39.3° Z_0 = 24.4 ohms

ω = 13.45 x 10^9 radians/sec

Y_L = 0.0185 - j.00527 (matched 50Ω line)

ωL_V = 1.658 ohms

ωC_A = 0.066 mhos

ωL_ℓ = 14.29 ohms

Upon solving Eq 4.13 to find the wave length for which the shunt susceptance is zero, we find λ_{res} to be 13.95 cm. Since the values of shunt conductance and external Q vary slowly with wave length, we use the quantities calculated above (at 14 cm) for the numerical solutions to Eqs 4.12 and 4.18. The results are

$$\frac{1}{G_{shunt}} = 1835 \text{ ohms} ; \qquad Q_e = 160$$

The experimental values for resonant wave length of the cavity in the absence of the cathode are 13.864 cm and 13.786 cm for the Model 7A No. 33 and the Model 7B No. 40, respectively. Results from Q measurements give external Q's of 340 for the No. 33 tube and 230 for the No. 40 tube.

The disagreement between the two experimental external Q's for the aforementioned tubes is at present unexplainable in terms of the tube geometries since both tubes have the same resonator dimensions. This discrepancy will be checked as soon as the tubes are available for measurements without cathodes. The discrepancy between measurement and theory is probably the result of oversimplification of the circuit used in the analysis. Further work on the analysis of the resonator is contemplated.

7. CATHODE STRUCTURES AND THE CATHODE-CIRCUIT PROBLEM

The Model 7 resonator system has been used in conjunction with a number of different cathodes, a few of which are shown in Fig. 7.1. Fig. 7.1(a) shows a thoriated tungsten bifilar helix cathode, which was used at an early stage of tube development. Operation with this cathode resulted in a power loss through the cathode line and poor oscillator performance. The cathode shown in Fig. 7.1(b) differs from that of Fig. 7.1(a) mainly in the increased diameter of the cathode stem. The enlarged section of the cathode stem, together with the inner surface of one of the pole pieces, forms a quarter-wave cathode-line by-pass. This by-pass makes the potential difference between the cathode and the bar anodes much smaller than the potential difference between the cathode and the vanes.

The r-f voltage unbalance for the Model 7A No. 33 tube is conservatively estimated to be over twenty-five to one. The reactance of the $\lambda/4$ cathode-line by-pass is much less than the Z_0 of the by-pass over a wide frequency range. The Z_0 for the by-pass is 4.05 ohms. The capacitance between the vanes and the cathode was computed on the basis of a flux plot giving a resultant reactance at 14 cm of 204 ohms.

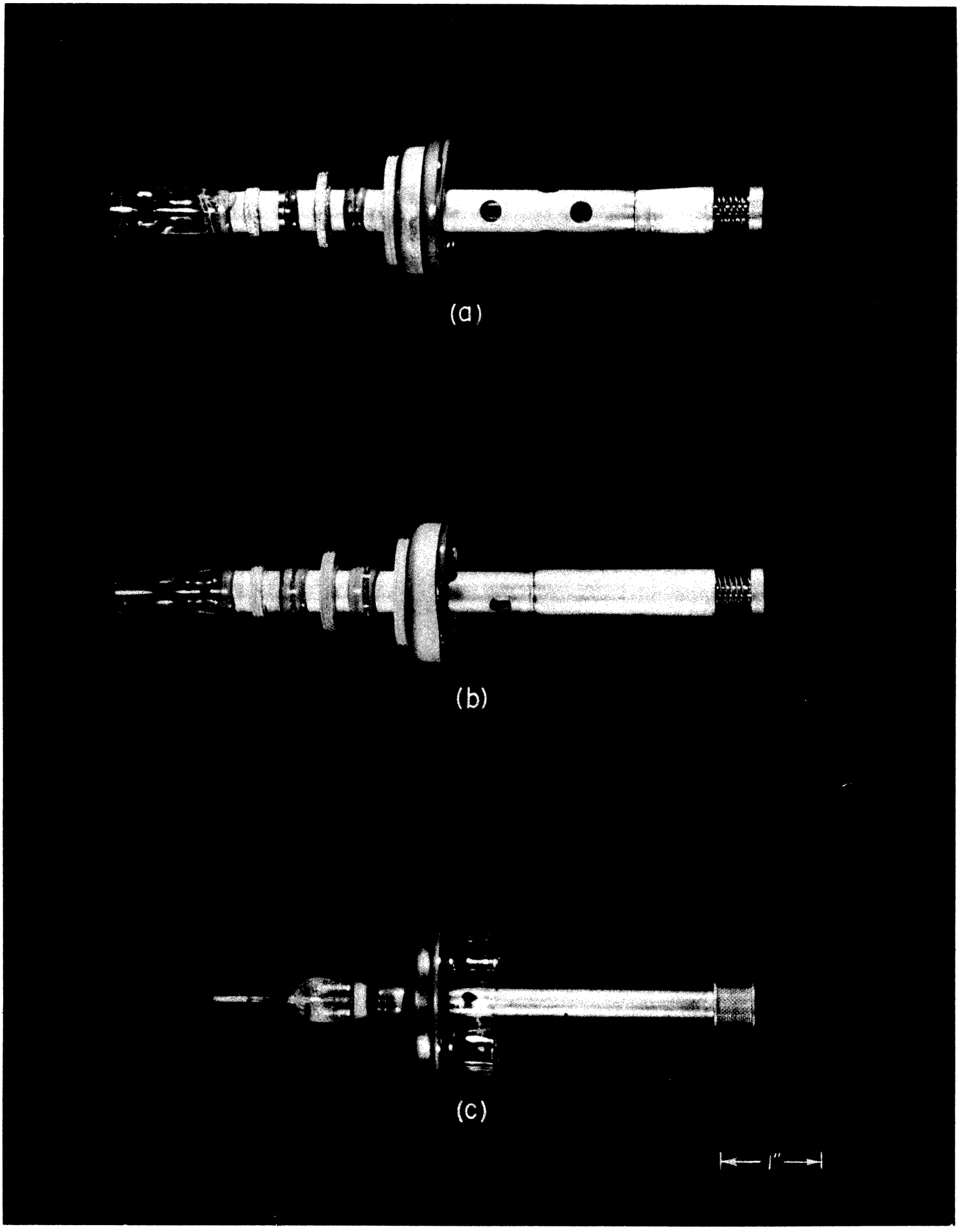

FIG. 7.1 CATHODES USED IN MODEL 7 TUBES

The use of the cathode-line by-pass reduces the power leakage through the cathode line but at the same time produces the aforementioned unbalance by placing a low reactance between the cathode and the inner wall of the center conductor, which, in turn, is directly connected to the bar anode segments. Fig. 7.2(a) shows the approximate space-charge-free r-f field distribution which would result from a geometry in which the cathode is at a potential midway between the anode segements of opposite phase (in the π mode). Fig. 7.2(b) shows the field distribution for the opposite limiting case, in which the cathode is at the same r-f potential as the bar anode segments.

Experimental results indicate that it is possible to achieve good electronic efficiency (with thoriated tungsten bifilar helix cathodes) even though an appreciable r-f voltage unbalance exists between the cathode and the anode segments of opposite phase. The maximum-current boundary for the tubes built so far is, however, not as great as it should be with the available cathode emission.

Rather unusual effects on maximum-current boundary, efficiency, and wave length are noticed near the magnetic field which corresponds to the cyclotron field, which is given by

$$B = 2\pi f \frac{m}{e} \qquad (7.1)$$

It is suspected that this behavior is related to the r-f voltage unbalance which exists in the interaction space of the structure. Operation is normal at magnetic fields well above the cyclotron field, as may be seen from the C-W performance charts given in Section 9, Experimental Results.

Fig. 7.1(c) shows a nickel-mesh oxide-coated cathode which is used in conjunction with a modified bar-and-vane geometry. The modified

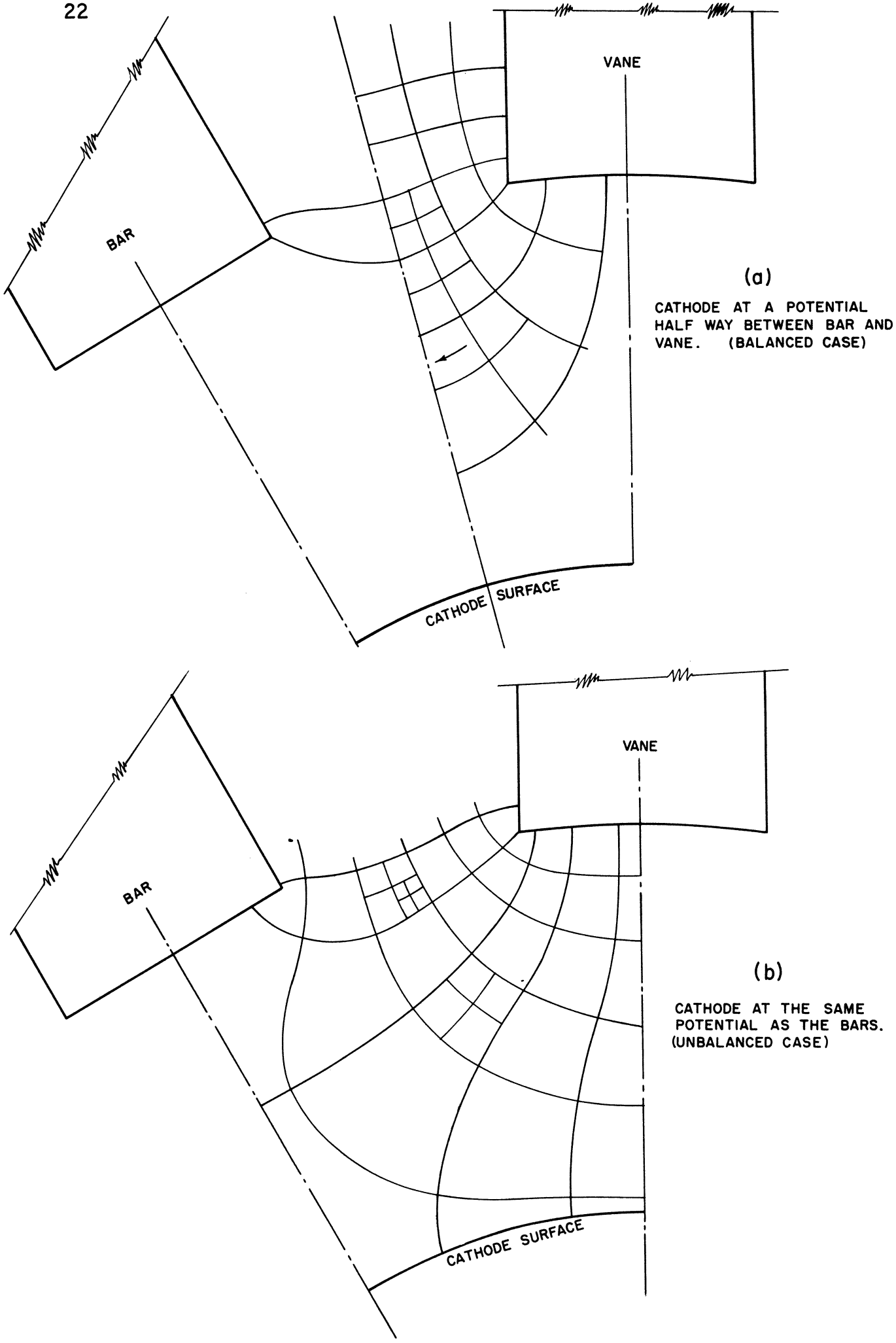

FIG. 7.2 SPACE CHARGE FREE R-F FIELD DISTRIBUTIONS SHOWING THE EFFECT OF CATHODE UNBALANCE.

DWG. NO. A

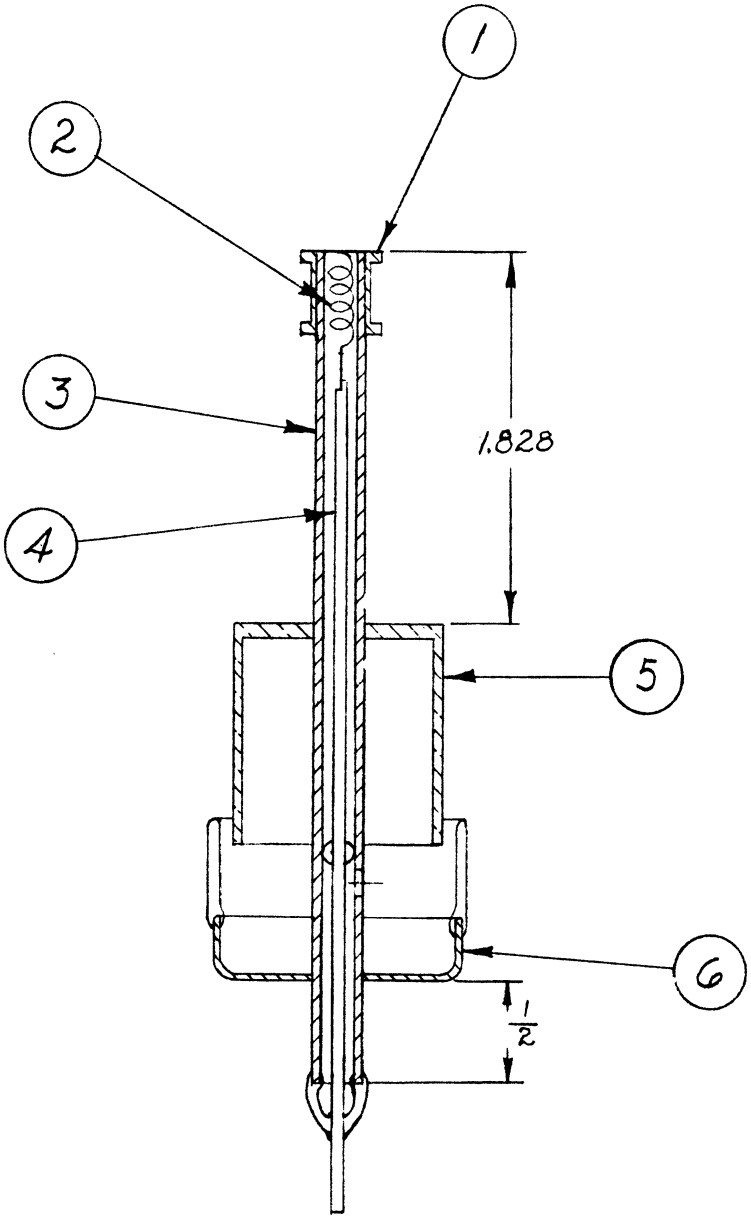

FIG. 7.3

. DIMENSIONS UNLESS OTHERWISE SPECIFIED MUST BE HELD TO A TOLERANCE - FRACTIONAL ± 1/64," DECIMAL ± .005," ANGULAR ± ½°

ENGINEERING RESEARCH INSTITUTE UNIVERSITY OF MICHIGAN ANN ARBOR MICHIGAN		DESIGNED BY JRB	APPROVED BY
		DRAWN BY MM	SCALE FULL
		CHECKED BY	DATE 11-7-50
PROJECT M-762		TITLE OXIDE COATED CATHODE	
CLASSIFICATION		DWG. NO. A- 8015	

UE | DATE

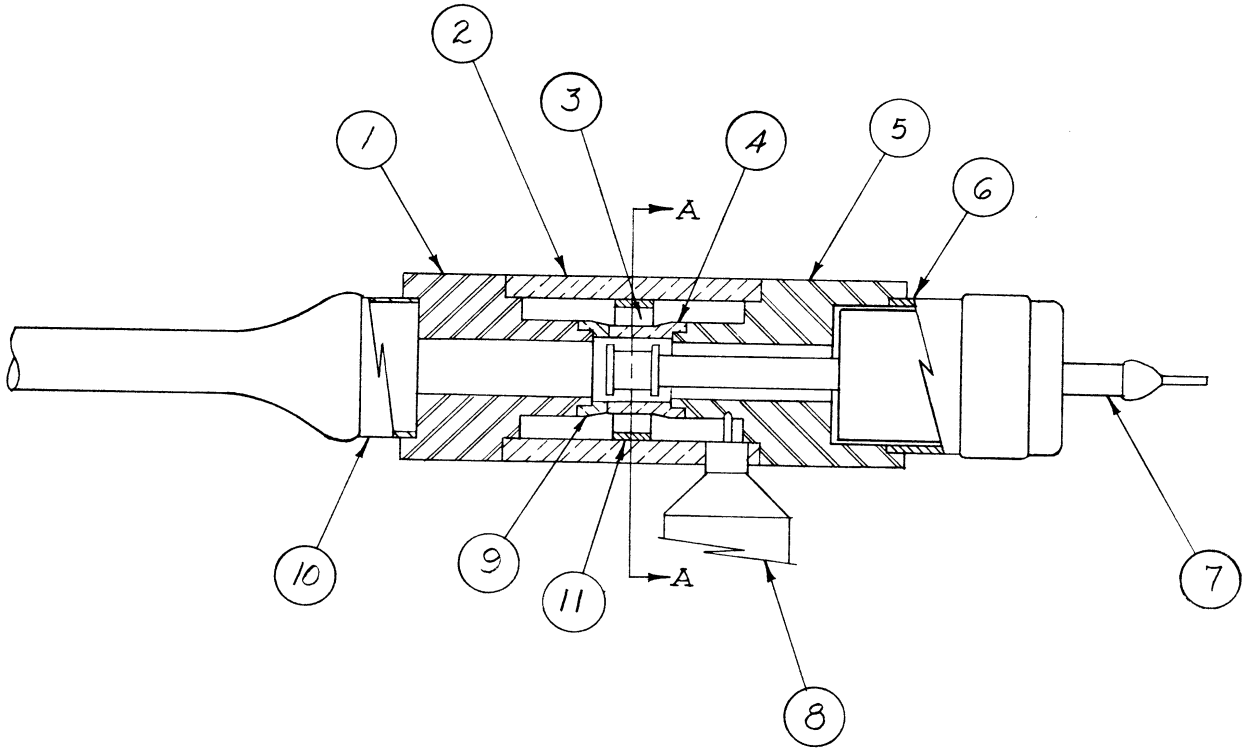

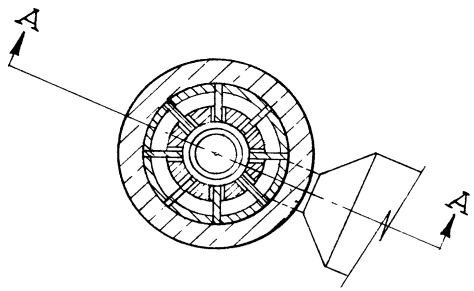

SECTION A-A

FIG. 7.4

1"

ALL DIMENSIONS UNLESS OTHERWISE SPECIFIED MUST BE HELD TO A TOLERANCE: FRACTIONAL ± 1/64," DECIMAL ± .005," ANGULAR ± ½°

ENGINEERING RESEARCH INSTITUTE UNIVERSITY OF MICHIGAN ANN ARBOR MICHIGAN		DESIGNED BY [illegible]	APPROVED BY
		DRAWN BY [illegible]	SCALE FULL
		CHECKED BY [illegible]	DATE 11-13-50
PROJECT M-762		TITLE CO-AXIAL MAGNETRON MODEL 7C	
CLASSIFICATION		DWG. NO. B-10,007C	
ISSUE	DATE		

DWG. NO. B

bar-and-vane geometry (see Appendix B) was designed for the purpose of achieving a better balance of r-f potential differences with respect to the cathode. The cathode stem, in this case, was made as small in diameter as possible in order to attain minimum capacitance to the inner wall of the center conductor.

Another oxide-coated cathode, an assembly of which is shown in Fig. 7.3, employs a choke and by-pass in the cathode line in order to provide a high impedance between the cathode and the center conductor. The cathode stem and inner wall of the center conductor form a quarter-wave choke beyond which a quarter-wave by-pass is formed by a copper cylinder closely spaced to an enlarged region of the center-conductor inner wall. An assembly drawing for this tube (Model 7C) is shown in Fig. 7.4. Pulsed data were obtained and are given in Section 9.

8. PARASITIC MODES

Experimental data on Model 7 structures employing thoriated tungsten cathodes indicate the presence of a higher order mode near 10 cm. This mode has been identified as a resonance existing in the vane anode segments similar to the ordinary mode of conventional vane magnetrons. The "vane mode" frequency is practically unaffected by cavity dimensions and is easily changed by altering the vane structure. This has been done for the tube shown in Fig. 1.1. A backing ring, part no. 6, shortens the vanes. The use of this ring changed the "vane mode" resonance from 11 cm to 9.6 cm without appreciably altering the 14-cm desired cavity mode.

In one tube (Model 7A No. 33), shown in Fig. 8.1, two outputs were provided: one for coupling to the desired 14-cm mode and one for

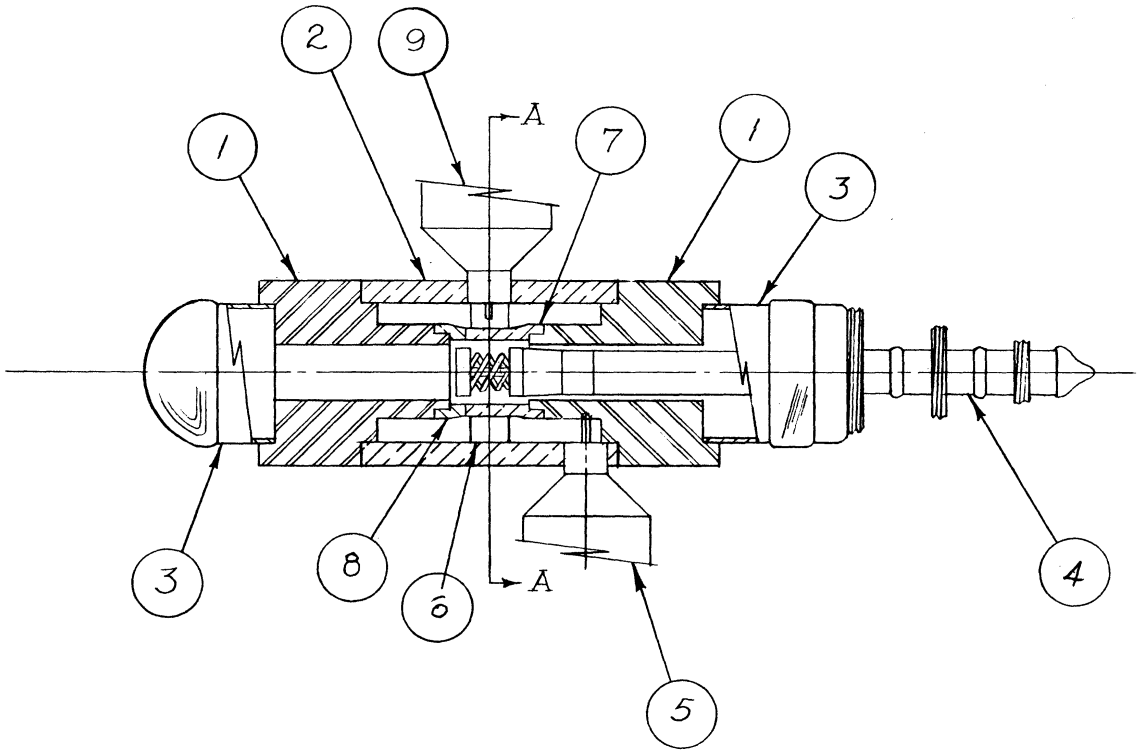

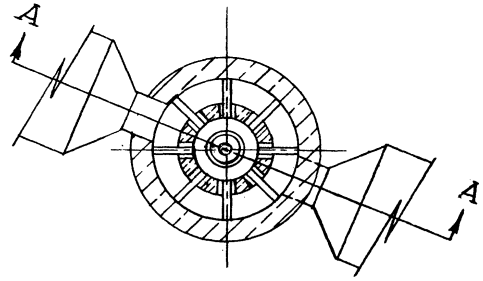

SECTION A-A

FIG. 8.1

1"

ALL DIMENSIONS UNLESS OTHERWISE SPECIFIED MUST BE HELD TO A TOLERANCE - FRACTIONAL ± 1/64," DECIMAL ± .005," ANGULAR ± ½°

		ENGINEERING RESEARCH INSTITUTE UNIVERSITY OF MICHIGAN ANN ARBOR MICHIGAN	DESIGNED BY H W W / APPROVED BY
			DRAWN BY / SCALE FULL
			CHECKED BY R E S / DATE
		PROJECT M-762	TITLE CO-AXIAL MAGNETRON MODEL 7A
1	7-20-50	CLASSIFICATION	DWG. NO. B- 10,007A
ISSUE	DATE		

DWG. NO. B-

coupling to the "vane mode". Thus, by selective loading of the two loops it was hoped that mode separation could be changed and effects on maximum-current boundary observed. Actually, the effect of loading does not seem to be sufficient to bring the two modes into competition. Mode separation is quite adequate, more than 30 per cent. The tube jumps completely out of oscillation in one mode before any oscillation is observed in the other. Data on the "vane mode" are given in Section 9 for one tube.

The tubes utilizing oxide-coated cathodes show the existence of not only the "vane mode" but also of a number of other modes. Little can be said about these extra modes until more complete information is available.

9. EXPERIMENTAL RESULTS

The experimental data reported in this section are not conclusive but are sufficient to indicate the results achieved thus far as well as the problems still to be solved. Table 9.1, which summarizes the performance of the tubes completed and tested up to this time, shows that power outputs of the order of 165 watts at good electronic efficiencies are attainable with this inherently unbalanced structure. The C-W performance charts of Figs. 9.1 through 9.4 show the maximum-current boundary encountered with tubes using thoriated tungsten cathodes. The reduced maximum-current boundary near the cyclotron magnetic field* is not considered serious, since operation at magnetic fields far removed from the cyclotron field is normal.

---

* This effect was also observed on another magnetron with the same interaction-space design but different resonant circuit. See the discussion of Model 4 in Section 2 of the interim report of December 15, 1949.

TABLE 9.1

SUMMARY OF MODEL 7 TUBE PERFORMANCE

Tube	Description *	Q_L	Q_o	Q_{ext}	λ_o	B gauss	E_b volts	I_b amps	P_o watts	Efficiency η %	η_{cir} %	η_e %
7A-33	Two output loops. Thoriated tungsten cathode, with $\lambda/4$ by-pass.	200	460	354	14.058	1390	3100	0.100	105	34	57	60
						1550	3530	0.092	150	46	57	81
7B-40	One output. Thoriated tungsten cathode with $\lambda/4$ by-pass. r_a/r_c decreased to 1.5.	211	1625	243	13.916	1390	2890	0.070	15	7.4	87	8.5
			Note: Cold-test data taken with dummy cathode made of solid nickel.			960	1740	0.100	220	11.5	87	13.1
7C-41	One output. Oxide-coated cathode with $\lambda/4$ choke and $\lambda/4$ by-pass.	176	790	226	13.772	Operated pulsed only. No d-c power.						
7D-42	One output. Thoriated tungsten cathode with $\lambda/4$ by-pass. Size of coupling loop is double that of all other models.	64.5	658	71.5	14.59 (?)	1390	3400	0.055	102	55	90	61
						1690	4300	0.070	165	55	90	61
						1690	4230	0.060	146	58	90	65
7E-45	One output. Oxide-coated cathode with small diameter stem. Modified bar-and-vane structure.					Operated pulsed only. No d-c power.						

* All tubes except the Model 7B-40 have an anode-to-cathode ratio of 1.75.

FIG. 9.1

PERFORMANCE CHART - COAXIAL SINGLE-CAVITY MAGNETRON

FUNDAMENTAL CAVITY MODE $\lambda \approx 14.10$ CM.

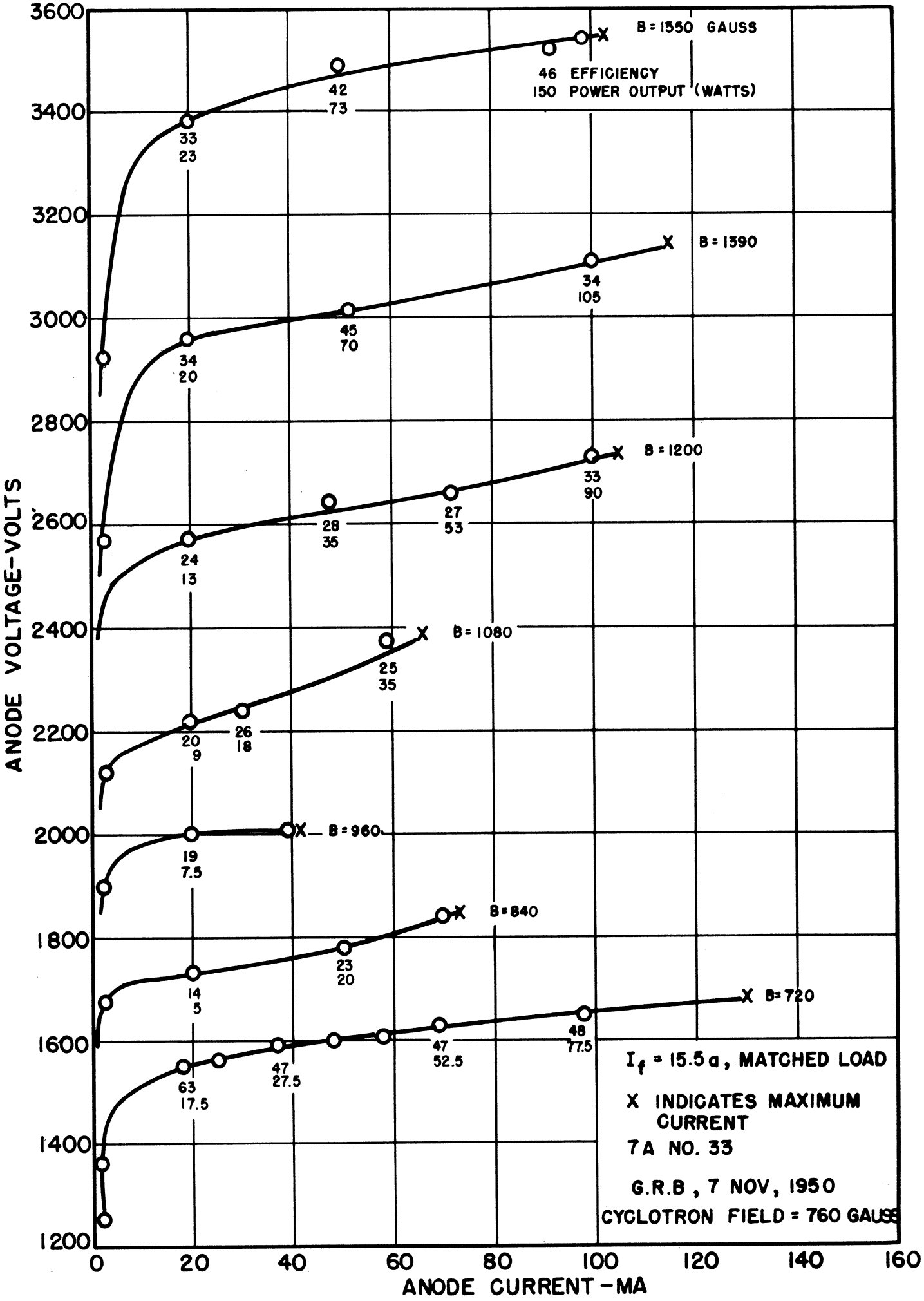

FIG. 9.2

PERFORMANCE CHART - COAXIAL SINGLE-CAVITY MAGNETRON

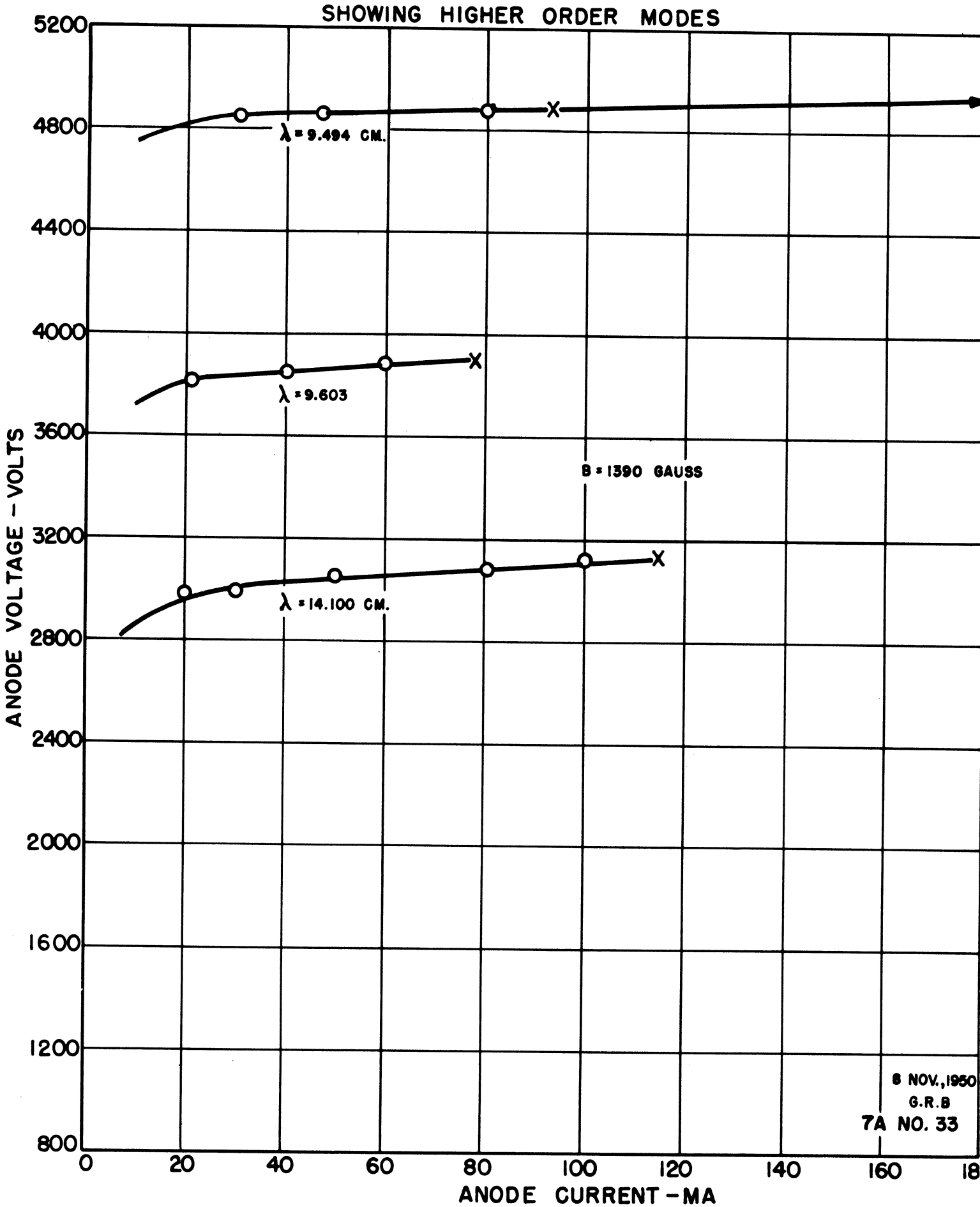

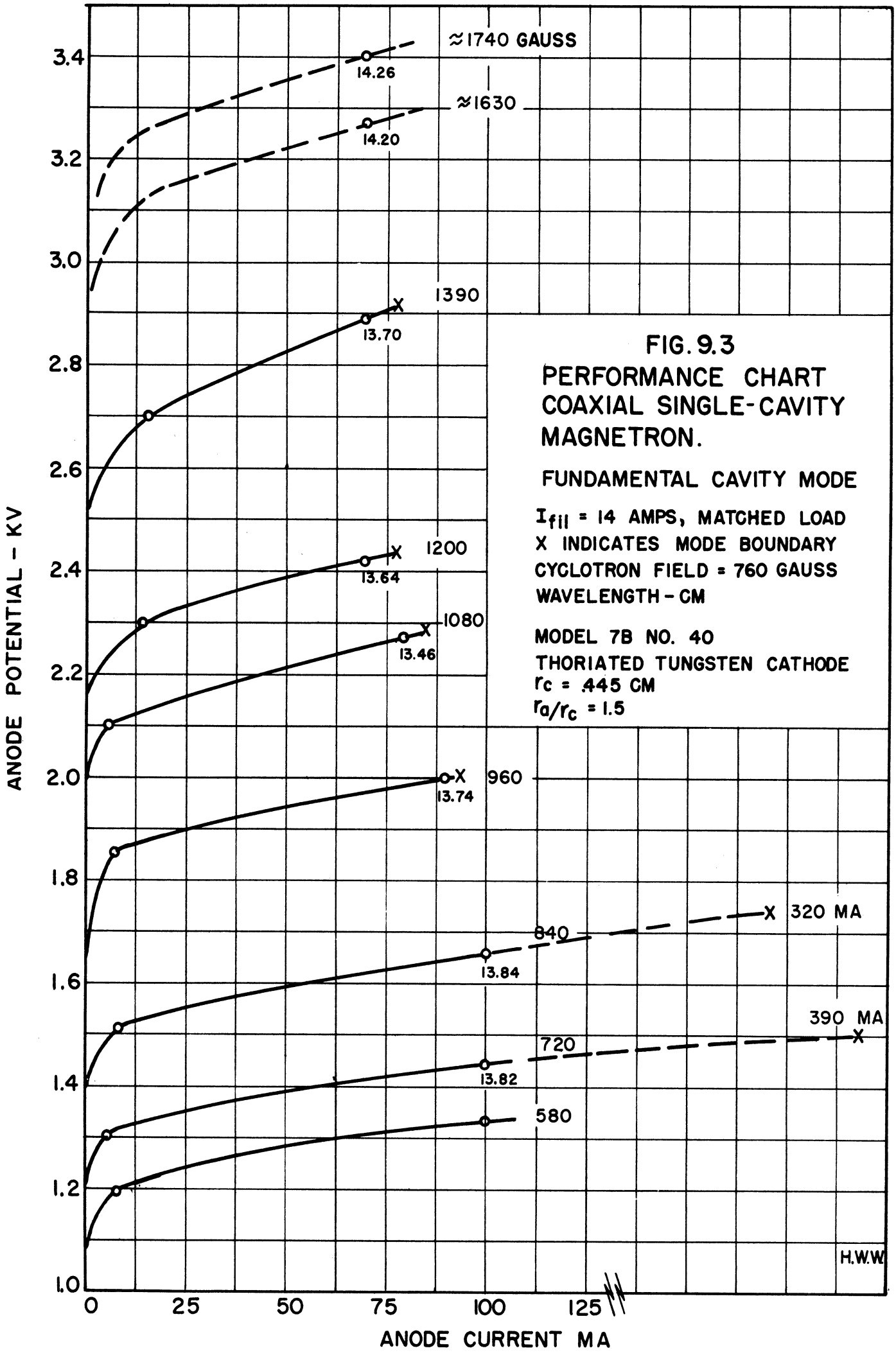

FIG. 9.3
PERFORMANCE CHART
COAXIAL SINGLE-CAVITY
MAGNETRON.

FUNDAMENTAL CAVITY MODE

I_{fil} = 14 AMPS, MATCHED LOAD
X INDICATES MODE BOUNDARY
CYCLOTRON FIELD = 760 GAUSS
WAVELENGTH - CM

MODEL 7B NO. 40
THORIATED TUNGSTEN CATHODE
r_c = .445 CM
r_a/r_c = 1.5

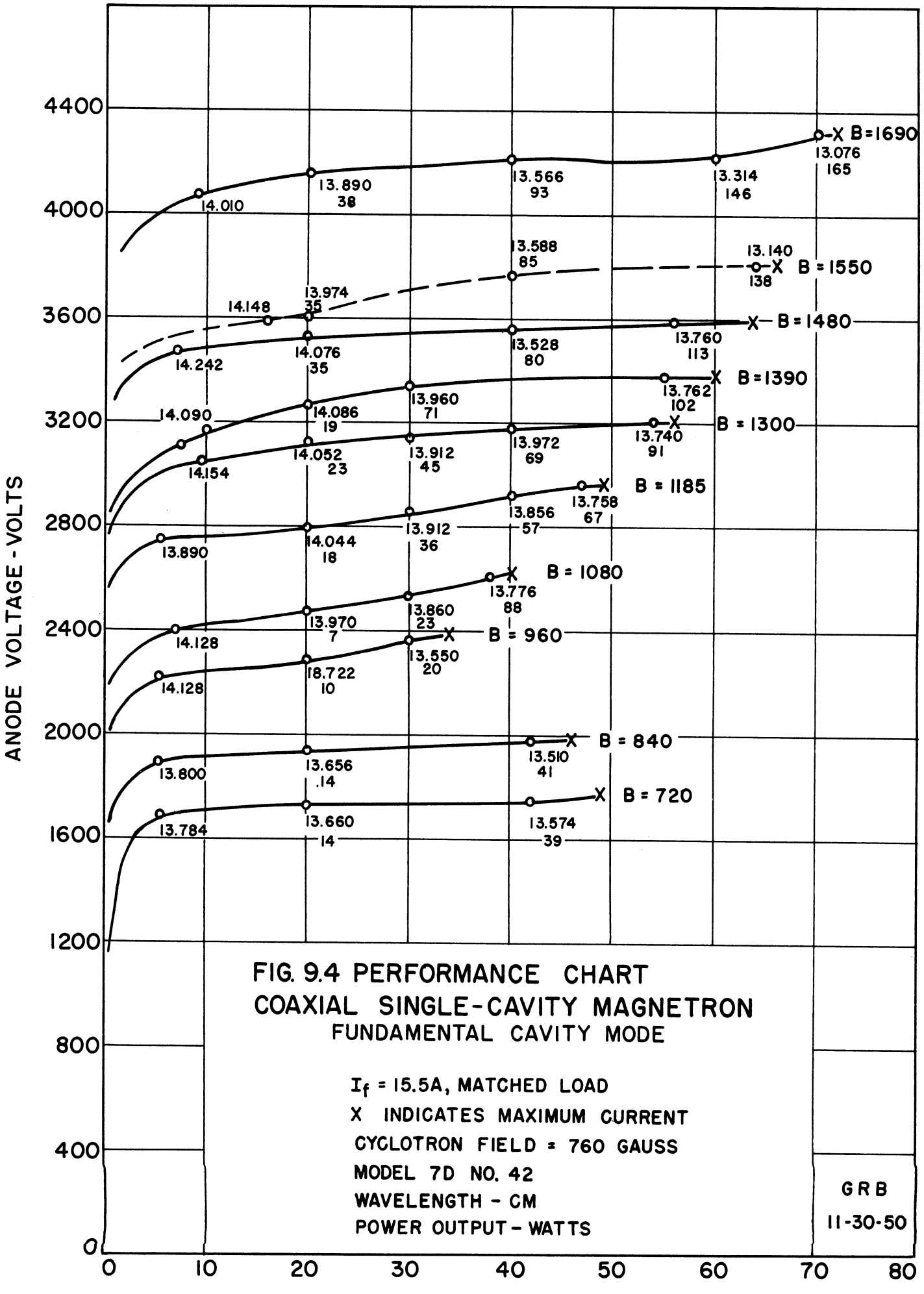

FIG. 9.4 PERFORMANCE CHART
COAXIAL SINGLE-CAVITY MAGNETRON
FUNDAMENTAL CAVITY MODE

I_f = 15.5A, MATCHED LOAD
X INDICATES MAXIMUM CURRENT
CYCLOTRON FIELD = 760 GAUSS
MODEL 7D NO. 42
WAVELENGTH - CM
POWER OUTPUT - WATTS

GRB
11-30-50

However, the maximum-current boundary is, in general, lower than would be expected in view of the available cathode emission. The question of how to increase the maximum-current boundary is one of the subjects of another investigation being carried on at this laboratory.*

A comparison of the performance chart of Fig. 9.3 with the other performance charts shows the effect of a change in interaction-space design on the maximum-current boundary. The anode-to-cathode radius ratio for the tube whose performance is given in Fig. 9.3 is 1.5, whereas the ratio for all other tubes built thus far has been 1.75. Since the amount of data available is very limited, any conclusions based on the comparison mentioned above cannot be considered as final.

Fig. 9.2 gives the performance for the Model 7A No. 33 tube, showing operation in modes other than the desired 14-cm resonator cavity mode and indicating the degree of mode separation. The lower wave length modes are both presumed to be "vane" modes.

The effects of heavier load on the operation of the Model 7 tubes are indicated in Fig. 9.4. The output coupling loop for this particular tube (Model 7D No. 42) is twice as large as that used in any of the other tubes. A power output of 165 watts at 55 per cent efficiency was obtained from this tube at a higher magnetic field and plate potential than those used for the Model 7A No. 33. It seems reasonable to expect that the power output from the latter tube would be greater than 165 watts if it were operated at the higher magnetic field. Comparison at the same magnetic fields shows that the Model 7A No. 33, in general, gives more power output, but at lower efficiency.

---

* See Technical Report No. 5.

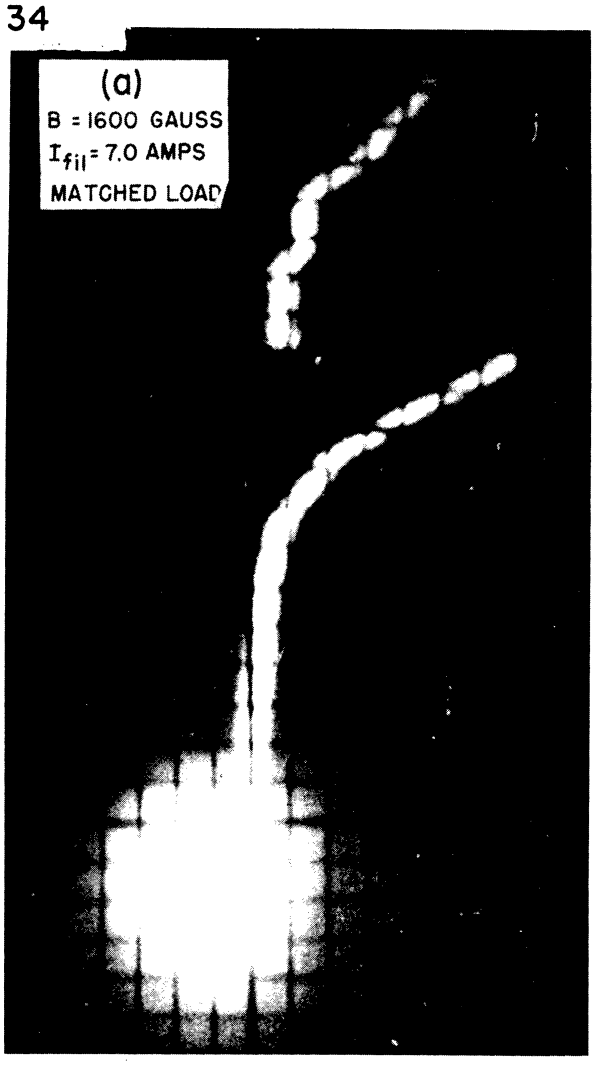

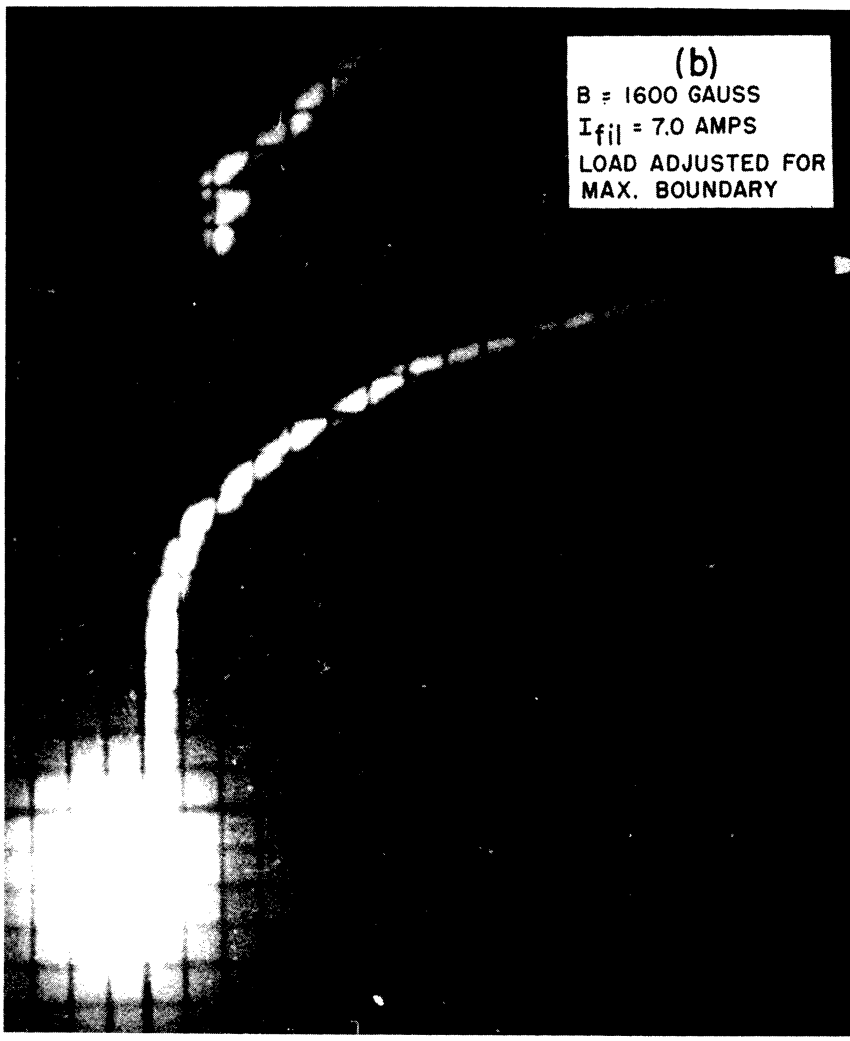

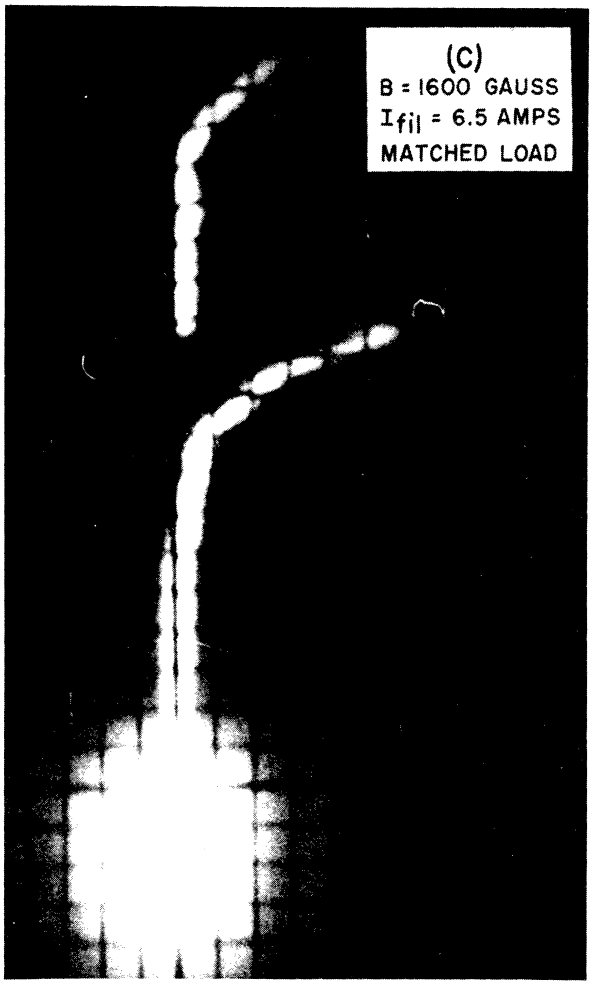

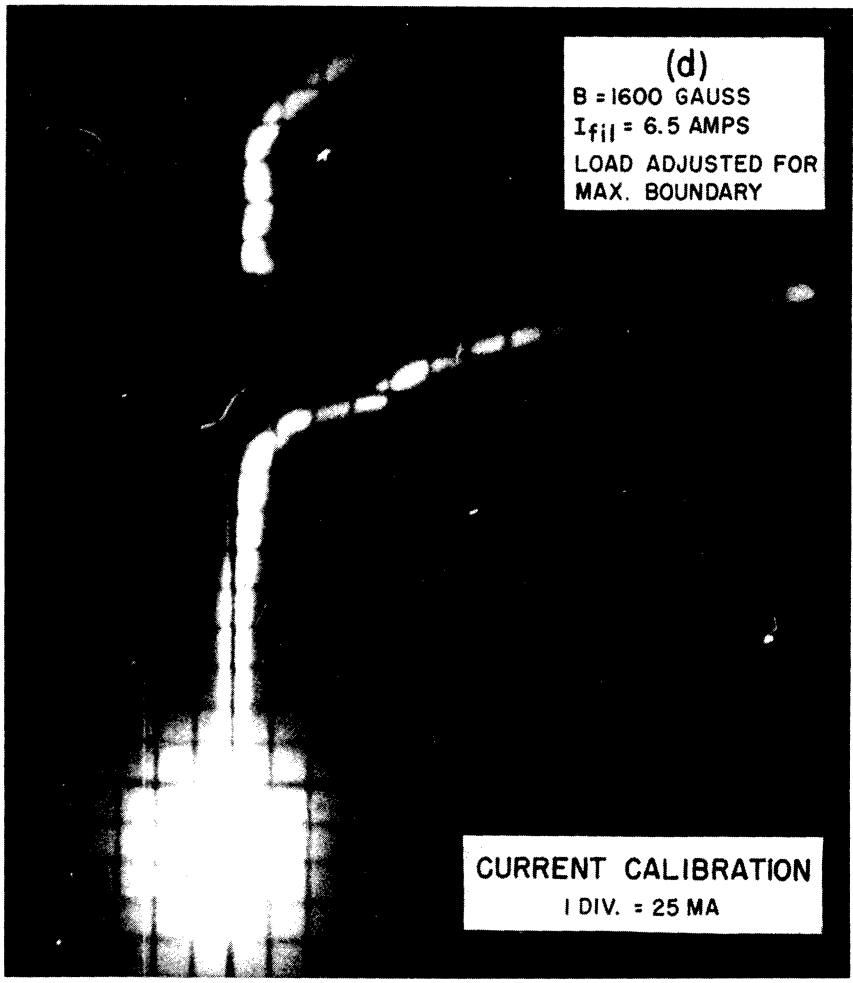

FIG. 9.5 PULSED PERFORMANCE FOR MODEL 7C NO. 41

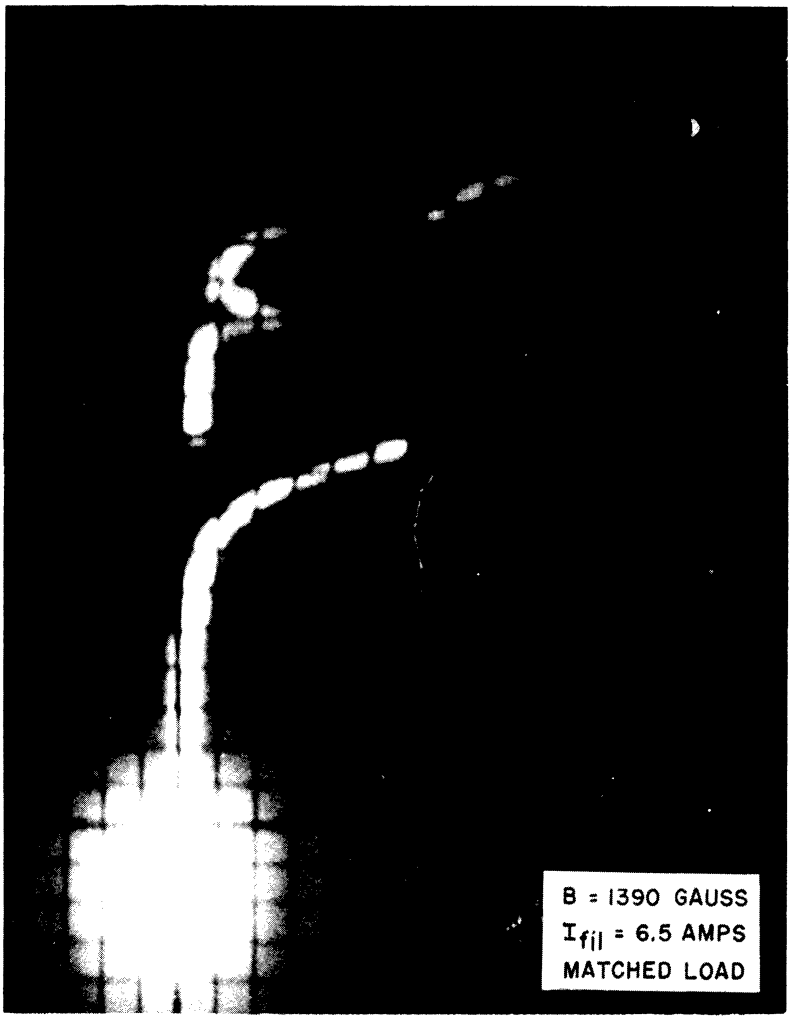

FIG. 9.6

PULSED PERFORMANCE FOR MODEL 7C NO. 41
(OXIDE CATHODE)

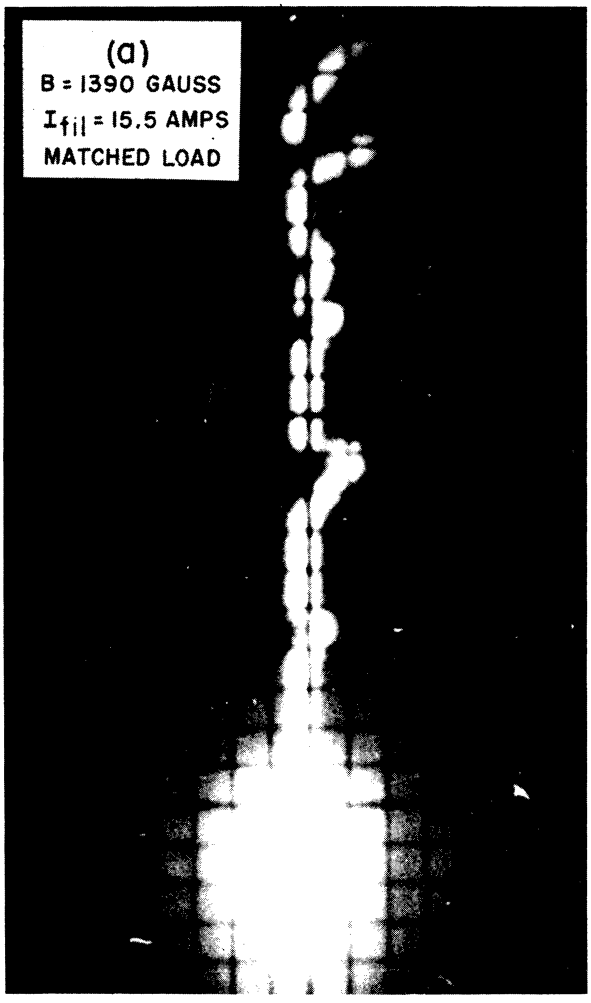

FIG. 9.7 PULSED PERFORMANCE FOR MODEL 7D NO. 42
(THORIATED TUNGSTEN CATHODE)

Oscillograms showing pulsed performance for two different tubes are given in Figs. 9.5 through 9.7, inclusive. These figures show the effect of load on maximum-current boundary and also indicate the presence of spurious modes of operation. The effect of cathode temperature on leakage current and maximum-current boundary is indicated in the pictures of Fig. 9.5. The current calibration (25 ma per division) is the same for all oscillograms.

Tubes employing oxide-coated cathodes have been tested under both pulsed and C-W operation. The C-W power output from these structures has been of the order of five to ten watts at very poor efficiencies. Further work with oxide-coated cathode magnetrons is required before any definite conclusions can be drawn as to the causes of the aforementioned poor operation.

10. CONCLUSIONS

The Model 7 single-cavity resonator magnetron has been shown to be capable of producing significant power output at good efficiencies It is relatively simple to construct, and the resonator can easily be designed for wide-range tunability. The basic geometry of the structure is readily adaptable to external-cavity magnetron construction as well as to parallel operation of anode structures. Resonator shapes and dimensions can be varied over a wide range without requiring a change in interaction-space design.

Performance of tubes constructed and tested so far indicates the necessity of further development in order to attain (a) greater maximum-

current boundary, and (b) a more complete understanding of the cathode-leakage problem and the effects of cathode unbalance. These subjects may or may not be directly related to each other. The C-W power-output limitation observed with magnetrons employing oxide-coated cathodes is of interest and also requires further investigation.

APPENDIX A

CALCULATION OF C_A AND L_V

APPENDIX A

CALCULATION OF C_A AND L_V

The use of field maps for calculations of bar-to-vane capacitance and of vane inductance is considered to be justified, since the dimensions of the vanes and bars are small relative to the wave length. The error incurred by considering the field distributions in two dimensions rather than in three dimensions is assumed to be greater than any field-mapping inaccuracies. The calculated bar-to-vane capacitance is probably correct to within ten per cent. This is a rough estimate because the answer is obtained on the basis of two-dimensional maps*. Calculations of vane inductance are based on the assumption of a uniformly distributed current density over the surface of the vane. This is, of course, only a very rough first approximation, since the edges of the vanes looking longitudinally into the coaxial line segments are essentially integral parts of the line terminations. The current density in the vanes should therefore be greater at these edges than anywhere else on the surface of the vanes. Although the distribution of current density is not directly available, we can obtain at least an order of magnitude by the approach used herein until a more detailed study of the true distribution can be made.

---

* Attwood, S. S., Electric and Magnetic Fields. 3rd ed., Chapter 7, Wiley and Sons, New York, 1949.

The capacitance is obtained from the two-dimensional maps by using the relation:

$$C = \varepsilon_o \frac{\text{Number of squares along an equipotential}}{\text{Number of squáres along a flux line}} .$$

(Capacitance is then in farads per meter measured perpendicularly into the paper.) The inductance is obtained by using the relation:

$$L = \mu_o \frac{\text{Number of squares along a magnetic equipotential line}}{\text{Number of squares along a magnetic flux line}} .$$

(Inductance is then in henries per meter measured perpendicularly into the paper.)

Computations

Vane-to-Bar Capacitance: From the map of Fig. A-1 we have:

$$C_o = \varepsilon_o \frac{7.75 \text{ squares}}{2 \text{ squares}} \quad \text{(farads per meter of map depth into the paper)} .$$

The map depth into the paper is equal to the vane height, which is 0.300 inch or 7.62×10^{-3} meter. Then:

$$C_1 = \varepsilon_o \frac{7.75}{2} \times 7.62 \times 10^{-3} \quad \text{(farads for one 22-1/2-degree section of the full sixteen-anode picture)} .$$

We now consider the top and bottom edge capacitance from the map of Fig. A-2.

$$C_{edge_o} = \varepsilon_o \frac{7.5}{2} \quad \text{(farads per meter of vane thickness)} .$$

Taking half the vane thickness as the dimension required in the 22-1/2-degree section in the map of Fig. A-1, and considering both the top and bottom edges of the vanes, we get:

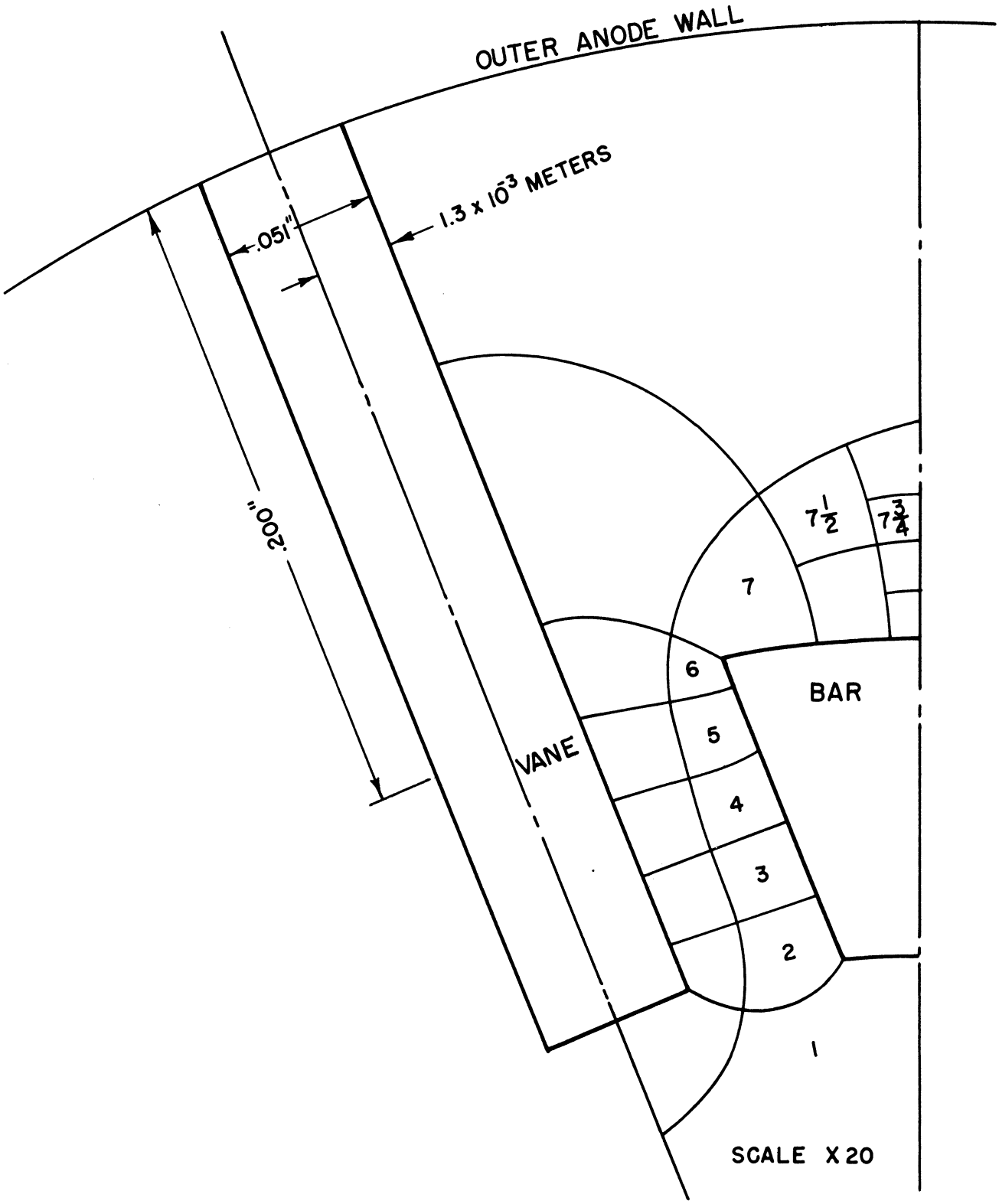

FIG. A-1
ONE SECTION OF THE MODEL 7A VANE-AND-BAR EXCITING STRUCTURE.

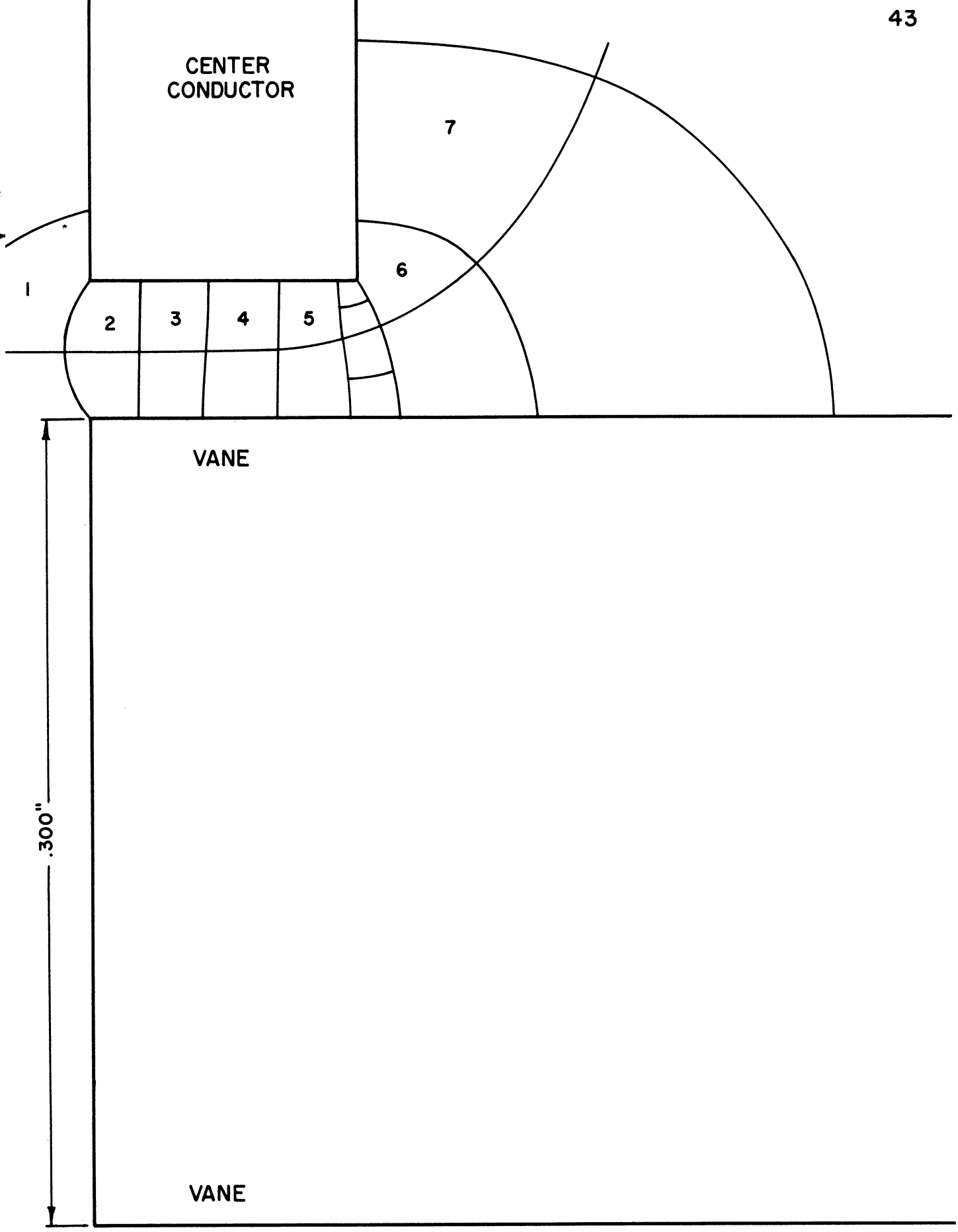

FIG. A-2

FLUX PLOT FOR THE COMPUTATION OF END CAPACITANCE BETWEEN VANES AND BARS

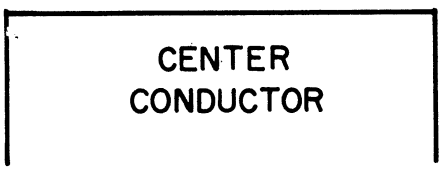

MODEL 7A SCALE X 20

$$C_{edge_1} = \varepsilon_o \frac{7.5}{2} \times 1.3 \times 10^{-3} \quad \text{(farads per 22-1/2-degree section)}$$

The total capacitance per 22-1/2-degree section, then, is:

$$C/\text{section} = C_1 + C_{edge_1} = 0.305\ \mu\mu f \ .$$

Since there are sixteen of these 22-1/2-degree sections in parallel for the complete system, we obtain;

$$C_A = 16\ (C_1 + C_{edge_1}) = 4.88\ \mu\mu f \ .$$

Vane Inductance: From the map of Fig. A-3, we obtain:

$$L_o = \mu_o \frac{4 \text{ squares}}{6.5 \text{ squares}} \text{ henries per meter of map depth (for 1/4 of the vane periphery)} .$$

Taking the entire periphery into account, we obtain:

$$L_1 = \frac{L_o}{4} \quad \text{(henries per meter of vane depth into the paper)}$$

Since the vane depth into the paper is approximately 0.200 inch or 5.08×10^{-3} meter, the inductance for one vane is

$$L_{v_1} = 5.08 \times 10^{-3}\ L_1 = 9.83 \times 10^{-10} \text{ henries}$$

The total inductance for eight vanes in parallel is

$$L_V = \frac{L_{v_1}}{8} = 122.9\ \mu\mu \text{henries}$$

Note: The distance between adjacent vanes has been taken as the average for the map of Fig. A-3.

FIG. A-3 FLUX PLOT FOR THE CALCULATION OF VANE INDUCTANCE

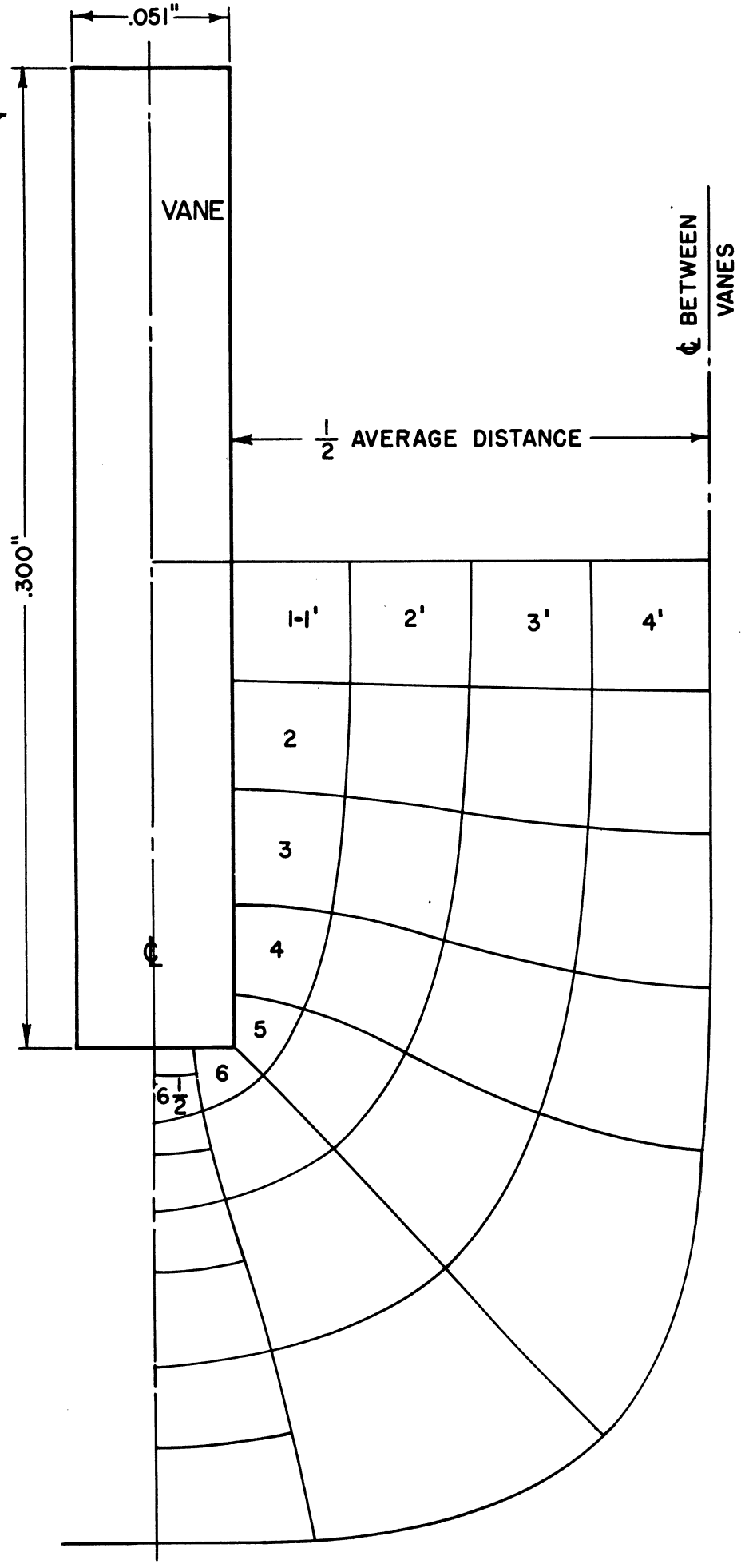

APPENDIX B

MODIFIED BAR AND VANE DETAILS

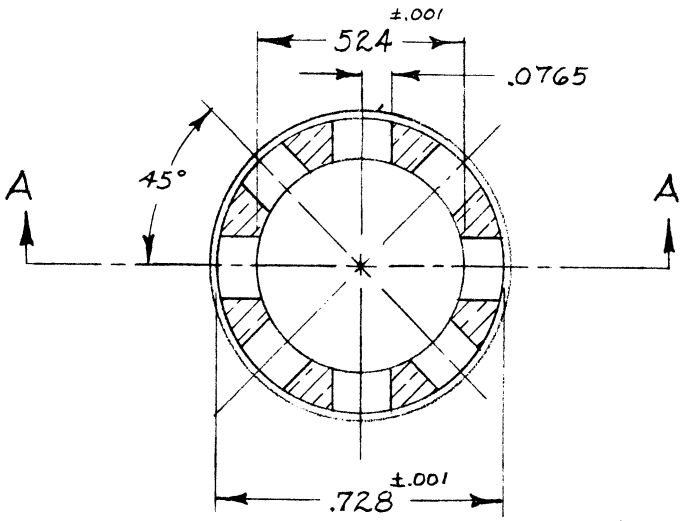

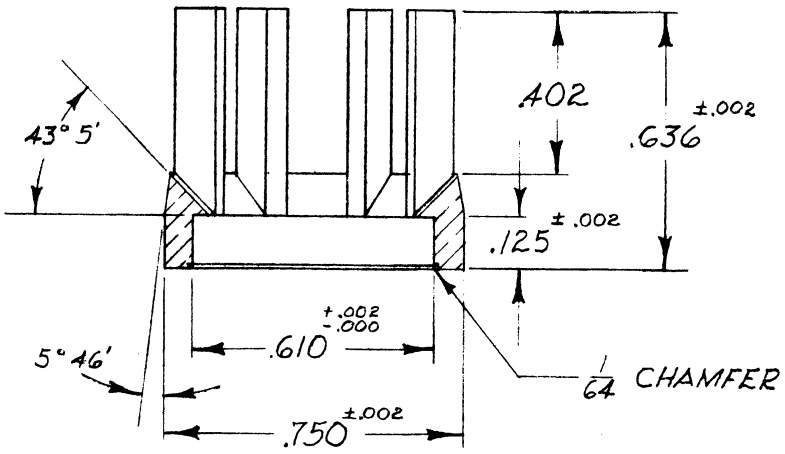

SECTION A A

OFHC COPPER 1 REQ'D

ALL DIMENSIONS UNLESS OTHERWISE SPECIFIED MUST BE HELD TO A TOLERANCE - FRACTIONAL ± 1/64," DECIMAL ± .005," ANGULAR ± ½°

ISSUE	DATE	ENGINEERING RESEARCH INSTITUTE UNIVERSITY OF MICHIGAN ANN ARBOR MICHIGAN	DESIGNED BY H [illegible]	APPROVED BY
			DRAWN BY MM	SCALE 2X
			CHECKED BY [illegible]	DATE 12-1-50
		PROJECT M-762	TITLE OSCILLATOR FINGERS	
		CLASSIFICATION	DWG. NO. A- 5025	

DWG. NO. A

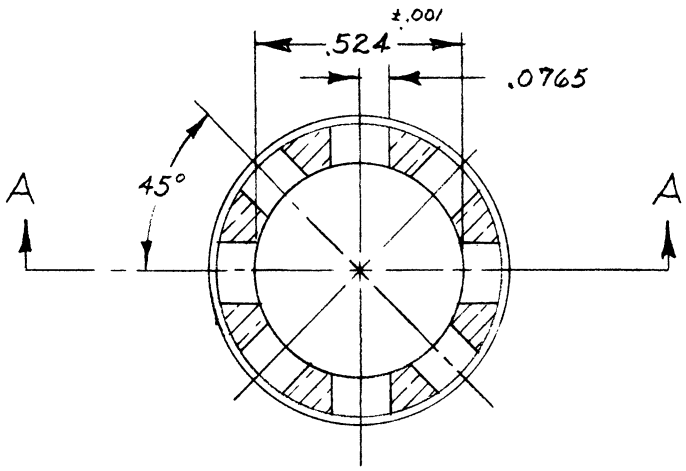

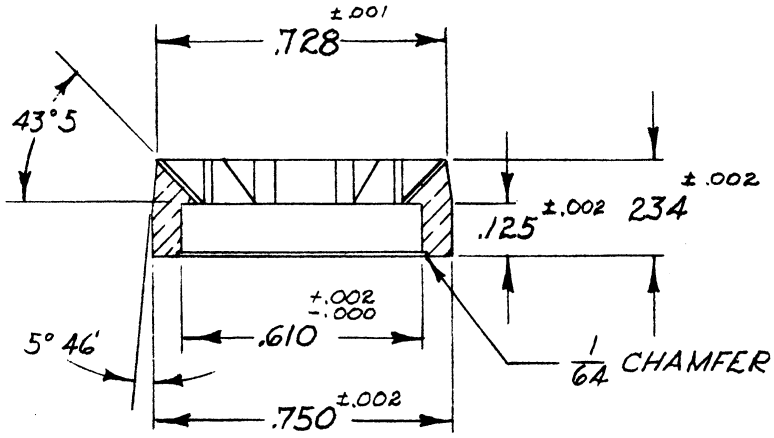

SECTION AA

OFHC COPPER

ALL DIMENSIONS UNLESS OTHERWISE SPECIFIED MUST BE HELD TO A TOLERANCE - FRACTIONAL ± 1/64," DECIMAL ± .005," ANGULAR ± ½°

ENGINEERING RESEARCH INSTITUTE UNIVERSITY OF MICHIGAN ANN ARBOR MICHIGAN		DESIGNED BY	APPROVED BY
		DRAWN BY MM	SCALE 2X
		CHECKED BY	DATE 12-4-50
PROJECT M-762		TITLE ANODE CAP	
CLASSIFICATION		DWG. NO. A- 5026	

ISSUE | DATE

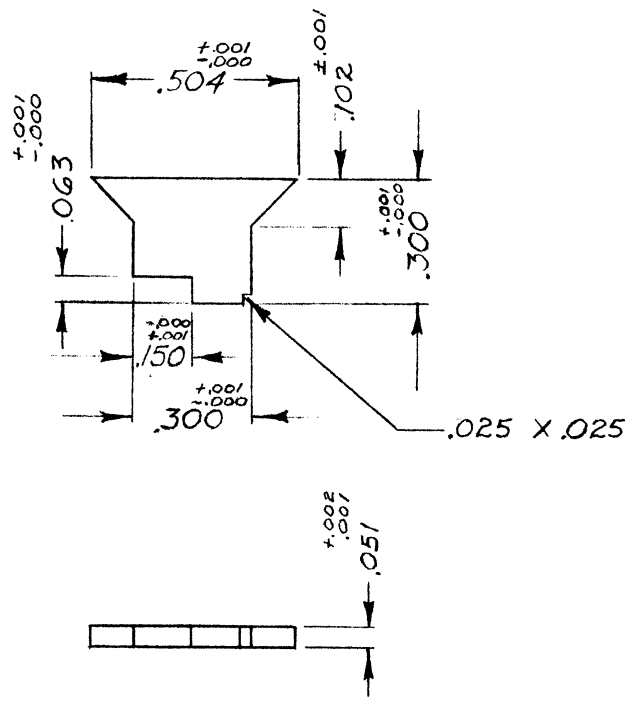

OFHC COPPER 8 REQ'D

ALL DIMENSIONS UNLESS OTHERWISE SPECIFIED MUST BE HELD TO A TOLERANCE - FRACTIONAL ± 1/64," DECIMAL ± .005," ANGULAR ± ½°

ISSUE	DATE			
		ENGINEERING RESEARCH INSTITUTE UNIVERSITY OF MICHIGAN ANN ARBOR MICHIGAN	DESIGNED BY [illegible]	APPROVED BY
			DRAWN BY [illegible]	SCALE 2 X
			CHECKED BY [illegible]	DATE 12-21-50
		PROJECT M-762	TITLE ANODE VANE	
		CLASSIFICATION	DWG. NO. A-5027	

DISTRIBUTION LIST

20 copies - Director, Evans Signal Laboratory
Belmar, New Jersey
FOR - Chief, Thermionics Branch

10 copies - Chief, Bureau of Ships
Navy Department
Washington 25, D. C.
Attention: Code 930A

10 copies - Director, Air Materiel Command
Wright-Patterson Air Force Base
Dayton, Ohio
Attention: Electron Tube Section

10 copies - Chief, Engineering and Technical Service
Office of the Chief Signal Officer
Washington 25, D. C.

2 copies - H. Wm. Welch, Jr., Research Physicist
Electron Tube Laboratory
Engineering Research Institute
University of Michigan
Ann Arbor, Michigan

1 copy - Engineering Research Institute File
University of Michigan
Ann Arbor, Michigan

W. E. Quinsey, Asst to the Director
Engineering Research Institute
University of Michigan
Ann Arbor, Michigan

W. G. Dow, Professor
Dept. of Electrical Engineering
University of Michigan
Ann Arbor, Michigan

Gunnar Hok, Research Engineer
Engineering Research Institute
University of Michigan
Ann Arbor, Michigan

J. R. Black, Research Engineer
Engineering Research Institute
University of Michigan
Ann Arbor, Michigan

G. R. Brewer, Research Associate
Engineering Research Institute
University of Michigan
Ann Arbor, Michigan

J. S. Needle, Instructor
Dept. of Electrical Engineering
University of Michigan
Ann Arbor, Michigan

Dept. of Electrical Engineering
University of Minnesota
Minneapolis, Minnesota
Attention: Prof. W. G. Shepherd

Westinghouse Engineering Laboratories
Bloomfield, New Jersey
Attention: Dr. J. H. Findlay

Columbia Radiation Laboratory
Columbia University Dept. of Physics
New York 27, New York

Electron Tube Laboratory
Dept. of Electrical Engineering
University of Illinois
Urbana, Illinois

Dept. of Electrical Engineering
Stanford University
Stanford, California
Attention: Dr. Karl Spangenberg

National Bureau of Standards Library
Room 203, Northwest Building
Washington 25, D. C.

Radio Corporation of America
RCA Laboratories Division
Princeton, New Jersey
Attention: Mr. J. S. Donal, Jr.

Dept. of Electrical Engineering
Pennsylvania State College
State College, Pennsylvania
Attention: Prof. A. H. Waynick

Document Office - Room 20B-221
Research Laboratory of Electronics
Massachusetts Institute of Technology
Cambridge 39, Massachusetts
Attention: John H. Hewitt

Bell Telephone Laboratories
Murray Hill, New Jersey
Attention: S. Millman

Department of Physics
Cornell University
Ithaca, New York
Attention: Dr. L. P. Smith

Special Development Group
Lancaster Engineering Section
Radio Corporation of America
RCA Victor Division
Lancaster, Pennsylvania
Attention: Hans K. Jenny

Magnetron Development Laboratory
Power Tube Division
Raytheon Manufacturing Company
Waltham 54, Massachusetts
Attention: Edward C. Dench

Vacuum Tube Department
Federal Telecommunication Labs, Inc.
500 Washington Avenue
Nutley 10, New Jersey
Attention: A. K. Wing, Jr.

Microwave Research Laboratory
University of California
Berkeley, California
Attention: Prof. L. C. Marshall

General Electric Research Laboratory
Schenectady, New York
Attention: Dr. Wilbur Hull

Cruft Laboratory
Harvard University
Cambridge, Massachusetts
Attention: Prof. E. L. Chaffee

Research Laboratory of Electronics
Massachusetts Institute of Technology
Cambridge, Massachusetts
Attention: Prof. S. T. Martin

Collins Radio Company
Cedar Rapids, Iowa
Attention: Robert M. Mitchell

Dept. of Electrical Engineering
University of Kentucky
Lexington, Kentucky
Attention: Prof. H. Alex Romanowitz

Dept. of Electrical Engineering
Yale University
New Haven, Connecticut
Attention: Dr. H. J. Reich

Document Office for Government Research
Contracts, Harvard University
Cambridge, Massachusetts
Attention: Mrs. Marjorie L. Cox